



Journal Homepage: [-www.journalijar.com](http://www.journalijar.com)

INTERNATIONAL JOURNAL OF ADVANCED RESEARCH (IJAR)

Article DOI:10.21474/IJAR01/20398
DOI URL: <http://dx.doi.org/10.21474/IJAR01/20398>



RESEARCH ARTICLE

YOLOV10 AND SAM 2.1 FOR ENHANCED MRI SEGMENTATION AND IMPROVED NEUROLOGICAL DISEASE DIAGNOSIS

Anand Ratnakar¹, Suraj Sawant² and Jayant Karajagikar¹

1. Dept. of Manufacturing Engineering and Industrial Management, COEP Technological University Pune, India.
2. Dept. of Computer Science & IT, COEP Technological University Pune, India.

Manuscript Info

Manuscript History

Received: 11 December 2024
Final Accepted: 14 January 2025
Published: February 2025

Key words:-

Neurological Disease Diagnosis, MRI Imaging, YOLOv10, Segment Anything Model (SAM), Medical Image Segmentation, Explainable AI (XAI)

Abstract

Early and accurate diagnosis of neurological diseases through MRI imaging is crucial for effective treatment and patient management. This study presents a deep learning-based approach utilizing a diverse dataset of 12,121 MRI images spanning 12 categories across three major neurological diseases including Brain Tumor Disorders, Alzheimer's Disease and Parkinson's Disease. The dataset was structured into 9,894 images for training and 2,227 for validation. Six YOLOv10 variants (N, S, M, B, L and X) were employed for multi-class classification and localization with the YOLOv10-X model achieving the highest diagnostic accuracy. To enhance interpretability the Segment Anything Model (SAM) 2.1 was applied for post-detection segmentation generating precise masks over detected regions further refined with plasma colormap visualization. Comparative evaluations highlight notable improvements in diagnostic performance demonstrating the effectiveness of integrating segmentation and explainable AI. This research contributes to the development of an advanced interpretable AI-driven framework for neurological disease detection.

Copyright, IJAR, 2025,. All rights reserved.

Introduction:-

The early diagnosis of neurological disorders, including Brain Tumor Disorders, Alzheimer's Disease, and Parkinson's Disease, is crucial for timely intervention and improved patient outcomes. Magnetic Resonance Imaging (MRI) serves as a fundamental tool for detecting these conditions by providing high-resolution anatomical and pathological information. However, the manual interpretation of MRI images is time-consuming and subject to variability, underscoring the need for automated diagnostic solutions. Recent advancements in machine learning (ML) and deep learning have significantly enhanced medical image analysis, particularly in classification, object detection, and segmentation tasks [1, 2]. This study presents an advanced framework that integrates state-of-the-art object detection and segmentation models to improve the accuracy and efficiency of neurological disease diagnosis using MRI data.

Leveraging Deep Learning for Improved Diagnosis

Deep learning techniques have revolutionized medical imaging by enabling automated and accurate analysis of complex data. Object detection models such as the YOLO series have gained prominence for their speed and accuracy, while segmentation models like the Segment Anything Model (SAM) have improved interpretability through precise region identification [3, 4]. This study integrates six YOLOv10 models (N, S, M, B, L, and X) for

Corresponding Author:- Anand Ratnakar

Address:- Dept. of Manufacturing Engineering and Industrial Management, COEP Technological University Pune, India.

classifying MRI images into 12 classes, representing Brain Tumor Disorders, Alzheimer's Disease, and Parkinson's Disease. Further, the SAM 2.1 model enhances segmentation and interpretability, applying masks to detected bounding boxes and visualizing the results using plasma colormaps. By combining these advanced techniques, the framework aims to improve diagnostic precision and reliability.

Research Motivation and Proposed Approach

The increasing prevalence of neurological disorders, coupled with the need for accurate and explainable diagnostic systems, drives the motivation for this research. Traditional diagnostic methods heavily rely on radiologist expertise, which can be subjective and limited by human capacity [5]. In this study, a combined dataset of 12,121 MRI images is used, encompassing 12 distinct classes across three disorders. The YOLOv10 models are trained to perform multi-class classification and localization tasks, followed by segmentation using SAM 2.1. The interpretability of the results is enhanced through plasma colormap visualization, which aids in clinical decision-making by providing clear and interpretable outputs. The proposed approach addresses the challenges of traditional methods by integrating detection, segmentation, and explainable AI in a single framework.

Research Contribution

This study introduces a series of significant advancements in the field of medical imaging and neurological disease diagnosis:

1. A novel diagnostic framework integrating six YOLOv10 models for multi-class classification and localization of Brain Tumor Disorders, Alzheimer's Disease, and Parkinson's Disease across 12 distinct classes.
2. Utilization of the SAM 2.1 model for precise segmentation of detected bounding boxes, enhancing the interpretability of the results
3. Visualization of segmented regions using plasma colormaps, providing clearer insights for clinical decision-making.
4. Comprehensive evaluation of six YOLOv10 models on a diverse neurological MRI dataset, demonstrating the superior diagnostic accuracy of the YOLOv10-X model.
5. A unified methodology bridging object detection, segmentation, and explainable AI to create a robust, automated framework for medical applications.

This research represents a novel contribution to medical image analysis by presenting a multi-class classification and localization framework specifically tailored for neurological disease diagnosis. Unlike prior studies that focus on single conditions, this work encompasses the integrated diagnosis of three major neurological disorders, including 12 distinct classes. Through the application of six YOLOv10 variants, the YOLOv10-X model emerged as the most effective in handling the complexity of multi-class tasks.

Moreover, the inclusion of SAM 2.1 for post-detection segmentation, coupled with plasma colormap visualization, establishes a new standard for creating interpretable AI-driven diagnostic tools. To the best of our knowledge, this is the first attempt to apply a YOLO model to such a comprehensive dataset covering Brain Tumor Disorders, Alzheimer's Disease, and Parkinson's Disease, underscoring the innovation and potential impact of this work on clinical diagnostics.

Related Works

Brain tumor classification and segmentation presents several advanced methodologies and models. Nanda et al. [6] introduced a Saliency-K-mean-SSO-RBNN model, achieving high classification accuracies across multiple datasets. Saboor et al. [7] developed an AI-based CAD system using attention-gated recurrent units (A-GRU), which demonstrated superior accuracy on the BTB dataset. Srinivasan et al. [8] proposed three CNN models for multi-classification of brain tumors, each showing impressive detection and classification performance. Roy et al. [9] utilized a Dual-GAN mechanism in an ensemble-based pipeline, achieving notable accuracy in brain tumor classification. Khalighi et al. [10] reviewed the transformative role of AI in neuro-oncology, emphasizing its precision in brain tumor management.

Further advancements include Almufareh et al. [11] evaluating YOLOv5 and YOLOv7 models for segmentation and classification, with high precision and recall scores. Sarada et al. [12] presented a modified ResNet50V2 model, enhancing classification accuracy through various optimizations. Ashafuddula et al. [13] introduced ContourTL-Net for early-stage detection, achieving high sensitivity and specificity. Rajeswari et al. [14] developed the DFMN

model for severity prediction, demonstrating robust performance metrics. Zakariah et al. [15] proposed the Dual Vision Transformer-DSUNET model, achieving high Dice Coefficient values for segmentation tasks.

Musthafa et al. [16] combined ResNet50 with Grad-CAM for enhanced interpretability and accuracy in brain tumor detection. Yu et al. [17] introduced HSA-Net, which significantly improved segmentation and classification outcomes. Aboussaleh et al. [18] developed Inception-UDet, an improved U-Net architecture, achieving high Dice Similarity Coefficients. Malakouti et al. [19] utilized machine learning and transfer learning techniques, achieving high accuracies with LightGBM and GoogLeNet models. Yalamanchili et al. [20] proposed VGG-16 and EfficientNetB7 models, demonstrating high classification accuracy.

Priyadarshini et al. [21] proposed a fine-tuned EfficientNetV2S model for multigrade classification, achieving high precision and recall. Haque et al. [22] developed NeuroNet19, achieving high accuracy and robust performance metrics. Rasool et al. [23] introduced TransResUNet, combining ResNet U-Net with Transformer blocks for glioma segmentation, achieving high dice scores. Hossain et al. [24] proposed the IVX16 ensemble model, achieving high accuracy in multiclass classification. Finally, Iriawan et al. [25] combined YOLO and UNet architectures for effective detection and segmentation of MRI brain tumor images, achieving a high correct classification ratio.

Alzheimer's disease diagnosis and classification showcases several innovative approaches and models. Ozdemir and Dogan [26] developed a CNN model for early Alzheimer's diagnosis, achieving an impressive accuracy of 99.84% by integrating compression and excitation blocks, Avg-TopK pooling, and SMOTE to handle data imbalance. Biswas and Gini J [27] proposed a multi-class classification system using 3D MRI images, with the RandomForest classifier achieving 99% accuracy on the OASIS dataset. Ayus and Gupta [28] introduced hybrid models, CNN-Conv1D-LSTM and HReENet, for Alzheimer's identification, with HReENet achieving a remarkable 99.97% accuracy. Nour et al. [29] proposed a Deep Ensemble Learning (DEL) model using 2D-CNNs for diagnosing Alzheimer's via EEG signals, achieving 97.9% accuracy. Ali et al. [30] developed an integrated approach combining Improved Fuzzy C-means clustering and a hybrid CNN-LSTM classifier, achieving 98.13% accuracy.

Tripathy et al. [31] proposed an improved spatial attention guided depth separable CNN for Alzheimer's detection, achieving 99.75% accuracy on the OASIS dataset. Mahmood et al. [32] introduced the D3LM-LAN and MLM-MCSVM models for Alzheimer's classification, achieving up to 98.59% accuracy. Mahmud et al. [33] proposed an explainable AI-based approach using deep transfer learning and ensemble modeling, achieving up to 96% accuracy. Matlani [34] developed a hybrid BiLSTM-ANN model for early Alzheimer's diagnosis, achieving 99.22% accuracy on the ADNI dataset. Malu et al. [35] introduced CirMNet, a hybrid feature extraction technique, achieving 97.34% accuracy in Alzheimer's classification.

Bringas et al. [36] proposed CLADSI, a continual learning algorithm using accelerometer data, achieving up to 86.94% accuracy. Zia-ur-Rehman et al. [37] employed DenseNet-201 for Alzheimer's diagnosis using MRI scans, achieving 98.24% accuracy. Sorour et al. [38] proposed a CNN-LSTM model for early Alzheimer's detection using MRI data, achieving 99.92% accuracy. Yu et al. [39] integrated EEG signals and genetic data for Alzheimer's classification, with SVM achieving 92% accuracy. Song and Yoshida [40] applied Grad-CAM to a 3D-VGG16 network for Alzheimer's diagnosis using fMRI data, achieving 96.4% accuracy.

Alp et al. [41] proposed using Vision Transformer (ViT) for MRI processing in Alzheimer's diagnosis, achieving over 99% accuracy. Qian and Wang [42] developed MMANet for Alzheimer's classification and brain age prediction, achieving 96.02% accuracy. Finally, Mahim et al. [43] proposed a ViT-GRU model for Alzheimer's detection from MRI images, achieving up to 99.69% accuracy. These studies collectively highlight the advancements in AI and deep learning techniques for improving the diagnosis and classification of Alzheimer's disease.

Parkinson's disease diagnosis and classification presents several advanced methodologies and models. Magesh et al. [44] developed a machine learning model using LIME for early detection of Parkinson's from DaTSCAN images, achieving 95.2% accuracy. Bhandari et al. [45] integrated gene expression data with machine learning and explainable AI, identifying key gene biomarkers for Parkinson's diagnosis. Kumar et al. [46] utilized miRNA biomarkers and deep learning, achieving 95.65% accuracy in diagnosing Parkinson's. Priyadarshini et al. [47] combined 3D MRI imaging with Gradient Boosting, achieving 96.8% accuracy in Parkinson's detection. Yildirim et

al. [48] proposed a hybrid model (PDD-AOA-CNN) using sound data, achieving 98.19% accuracy in detecting Parkinson's.

Saleh et al. [49] developed a hybrid CNN-KNN ensemble classifier for predicting Parkinson's from hand sketching images, achieving 96.67% accuracy. Teo et al. [50] introduced a multilayer BiLSTM network with explainable AI to distinguish Parkinson's from essential tremor, achieving 90% accuracy. Islam et al. [51] integrated clinical assessments and neuroimaging data, achieving 98.44% accuracy with clinical data for Parkinson's detection. Veetil et al. [52] investigated data leakage in MRI-based Parkinson's classification using 2D CNNs, identifying VGG19 as the most robust model. Mahendran and Visalakshi [53] used ResNet50 for Parkinson's classification from spiral sketches, achieving 96.67% accuracy.

Palakayala and Kuppusamy [54] introduced AttentionLUNet for Parkinson's detection using MRI, achieving 99.58% accuracy. Yang et al. [55] applied deep learning to video of finger tapping for Parkinson's detection, achieving a test accuracy of 0.69. Wang et al. [56] proposed a deep learning method for cross-modality striatum segmentation using DaT SPECT and MR images, achieving strong performance metrics. Dentamaro et al. [57] investigated multimodal deep learning for early Parkinson's detection using the PPMI database, achieving 96.6% accuracy. Al-Tam et al. [58] proposed a stacking ensemble approach for Parkinson's diagnosis, achieving up to 96.18% accuracy. Desai et al. [59] developed a deep learning model using 3D MRI scans for Parkinson's classification, achieving 90.13% accuracy with data augmentation. These studies collectively highlight the advancements in AI and deep learning techniques for improving the diagnosis and classification of Parkinson's disease.

Materials and Methods:-

In this work, the workflow illustrated in Fig.1 is followed. The process for diagnosing neurological diseases using MRI images involves several structured steps. Initially, the MRI dataset, which includes 12 classes, is pre-processed by resizing, normalizing, and denoising the images. To enhance the dataset's robustness, data augmentations such as blurring, grayscale conversion, and contrast enhancement using CLAHE are applied [61].

Next, six versions of YOLOv10 models (N, S, M, B, L, X) are initialized with pre-trained weights and trained on the augmented dataset [60]. Following training, the models are rigorously evaluated using metrics like accuracy, precision, recall, mAP50, etc [61]. Post-training, the SAM 2.1-tiny model is utilized for segmentation, generating precise masks for the detected bounding boxes [62].

To interpret the results, colormap visualizations, such as plasma colormaps, are applied, providing insights into the model's decision-making process [61]. The final outputs include segmented and visualized predictions, which are validated to ensure accuracy and reliability [62]. This systematic approach integrates detection, segmentation, and interpretation for a comprehensive analysis of neurological diseases [61].

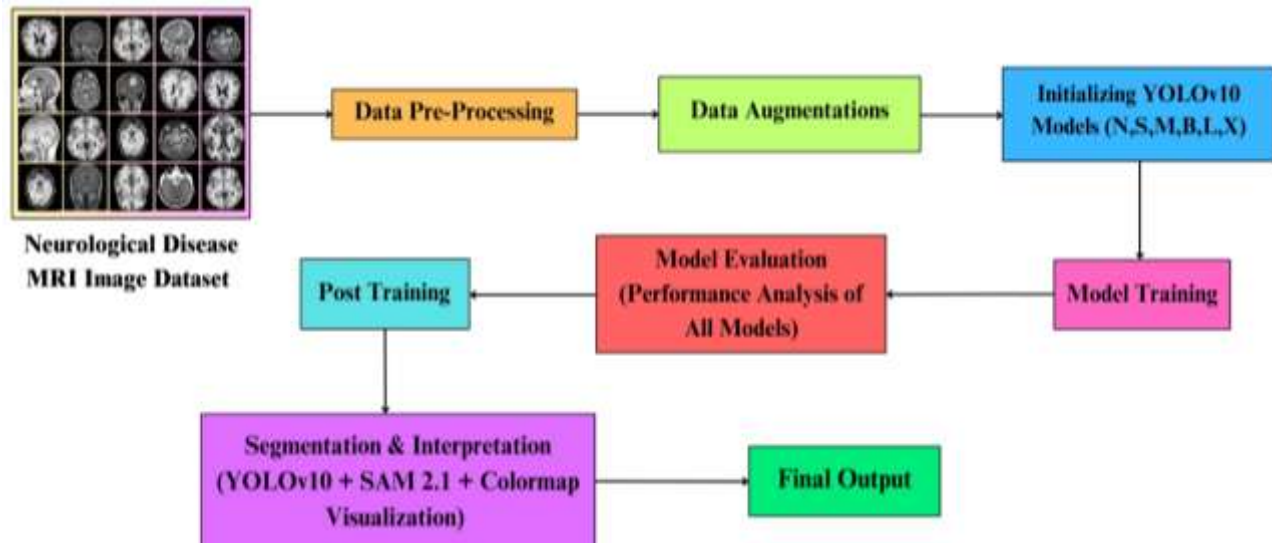


Fig.1:- Workflow of Proposed Methodology.

Neurological Disease MRI Image Dataset

The proposed Neurological Disease MRI Image Dataset, shown in Fig. 2, is a curated combination of three publicly available datasets sourced from Roboflow: the Brain Tumor Disorder Dataset [63], Alzheimer's Disease Detection Dataset [64], and Parkinson Disease Dataset [65]. This comprehensive dataset has been refined and pre-processed to meet the specific requirements of neurological disease classification, ensuring consistency and utility for the study.

The dataset comprises 12,121 MRI images categorized into 12 classes: 4 classes for Brain Tumor (Glioma, Meningioma, No Tumor, Pituitary), 5 for Alzheimer's Disease (Mild Demented, Moderate Demented, Non Demented, Severe Demented, Very Mild Demented), and 3 for Parkinson's Disease (PD Control, PD, Prodromal). The dataset attributes are detailed in Table 2. The data is split into 9,894 images (81.6%) for training and 2,227 images (18.4%) for validation, ensuring balanced model training and robust performance evaluation. This curated dataset provides a robust foundation for achieving high classification accuracy in the diagnosis of neurological diseases.

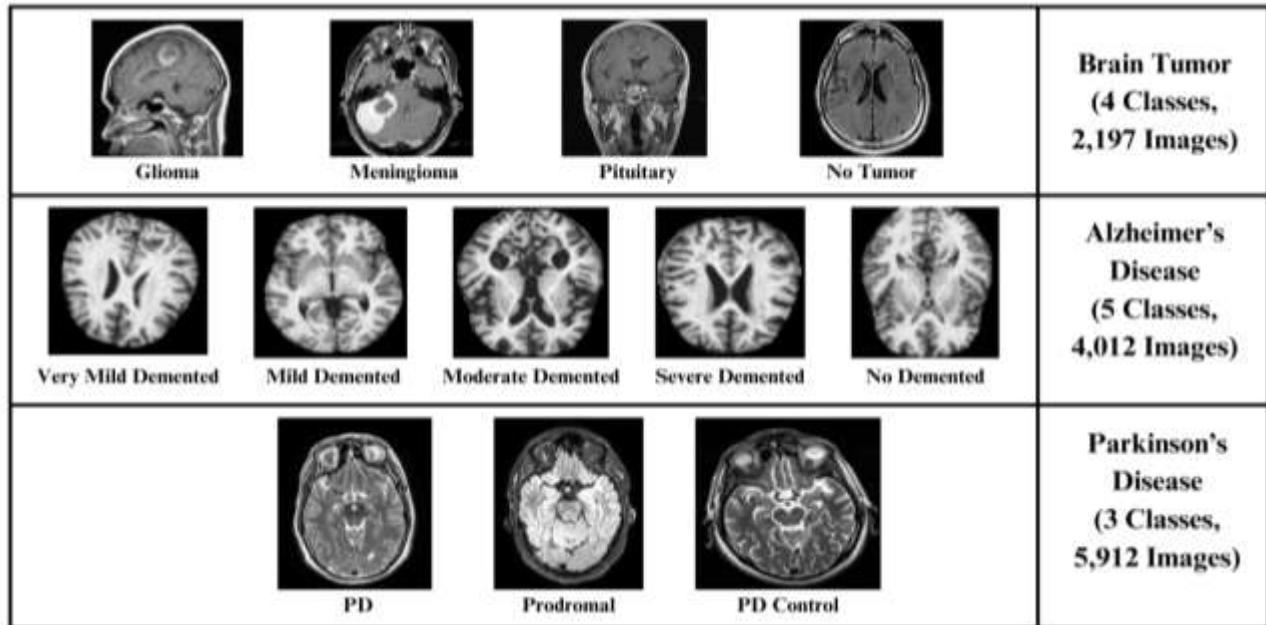


Fig. 2:- Neurological Disease MRI Image Dataset.

Index	Class	Index	Class
0	Glioma	6	Non Demented
1	Meningioma	7	Severe Demented
2	No Tumor	8	Very Mild Demented
3	Pituitary	9	PD Control
4	Mild Demented	10	PD
5	Moderate Demented	11	Prodromal

Table 1:- Details of Proposed Dataset Attributes.

Data Pre-Processing

To ensure the quality and uniformity of the MRI images while optimizing computational efficiency, the following pre-processing steps were applied:

- Resizing:** The original image dimensions (640 × 640 pixels) were resized to 320 × 320 pixels. This resizing was performed to reduce computational intensity while maintaining compatibility with YOLOv10 models [61].
- Normalization:** All pixel values were normalized to the range [0, 1], ensuring standardized data input and facilitating improved convergence during model training [60].
- Denoising:** Noise within the MRI images was reduced using Gaussian blur and median filtering techniques. These methods significantly enhanced image clarity, thereby improving the feature extraction capability of the YOLOv10 models [66].

Data Augmentations

As shown in Table 2, the following augmentation techniques were applied to enhance the robustness and generalizability of the models:

Augmentation Techniques	Significance
Blur Effects	Gaussian blur and median blur simulate variations in image quality.
Grayscale Conversion	Converts images to grayscale to emphasize structural features and reduce computational complexity.
Contrast Limited Adaptive Histogram Equalization (CLAHE)	Enhances image contrast while preventing over-enhancement.
Random Flipping and Rotation	Introduces variability in the dataset and reduces the risk of overfitting.

Table 2:- Data Augmentation Techniques and Their Significance [66-69].

YOLOv10 Models

As shown in Table 3, Six versions of YOLOv10 (N, S, M, B, L, and X) [84] were initialized with pre-trained weights for transfer learning to leverage feature representations learned from large datasets.

Model	Total No. Parameters	FLOPs (G)
YOLOv10-N	2.71 M (2,711,720)	8.4
YOLOv10-S	8.08 M (8,075,640)	24.8
YOLOv10-M	16.50 M (16,498,024)	64.0
YOLOv10-B	20.47 M (20,469,528)	98.8
YOLOv10-L	25.78 M (25,783,832)	127.3
YOLOv10-X	31.68 M (31,677,992)	171.1

Table 3:- An overview of YOLOv10 Models used in Proposed Work.

Results and Discussion:-

All YOLOv10 models were implemented on Google Colab using the Ultralytics version 8.3.51 framework, Python 3.10.12, and PyTorch 2.5.1+cu121. The experimental setup was equipped with a Tesla T4 GPU featuring 15,102 MB of memory and CUDA:0 acceleration. Model optimization was performed using the AdamW optimizer, with a learning rate of 0.000625 and a momentum value of 0.9 [70]. Each model underwent training for 50 epochs, with all input images resized to 320×320 for both training and validation.

The evaluation of YOLOv10 models was conducted using multiple performance metrics. Precision was utilized to assess the accuracy of positive predictions, while recall measured the model's capability to detect all relevant instances [71]. The F1-score, computed as the harmonic mean of precision and recall, provided a balanced performance assessment [72]. Additionally, detection accuracy was measured using mean Average Precision (mAP) at an Intersection over Union (IoU) threshold of 50% (mAP50) as well as across a range of IoU values from 50% to 95% (mAP50–95), offering comprehensive insights into model performance at varying overlap thresholds [73].

For computational efficiency analysis, the average latency per image was determined using the 2,227 images in the validation set. This metric quantified the average time required for the model to detect objects or classify instances within a single image, providing an important measure of inference speed and real-time applicability [74].

YOLOv10-N Model

The YOLOv10-N model, with the smallest architecture of 2.71 million parameters, achieved a precision of 86.89% and recall of 87.07%, resulting in an F1-Score of 86.98%. It attained a mAP50 of 89.94% and a mAP50–95 of 72.98%, with the lowest average latency of 25.1 milliseconds, making it computationally efficient for lightweight applications.

Table 4:- Performance Analysis for YOLOv10-N model.

Model	Image Size	Epochs	Total No. Parameters	FLOPs (G)	Precision (%)	Recall (%)	F1-Score (%)	mAP 50 (Val) (%)	mAP 50-95 (Val) (%)	Avg. Latency (Val) (ms)
YOLOv10-N	320	50	2.71 M (2,711,720)	8.4	86.89	87.07	86.98	89.94	72.98	25.10

Fig. 3:- Confusion Matrix (Normalized) for YOLOv10-N model.

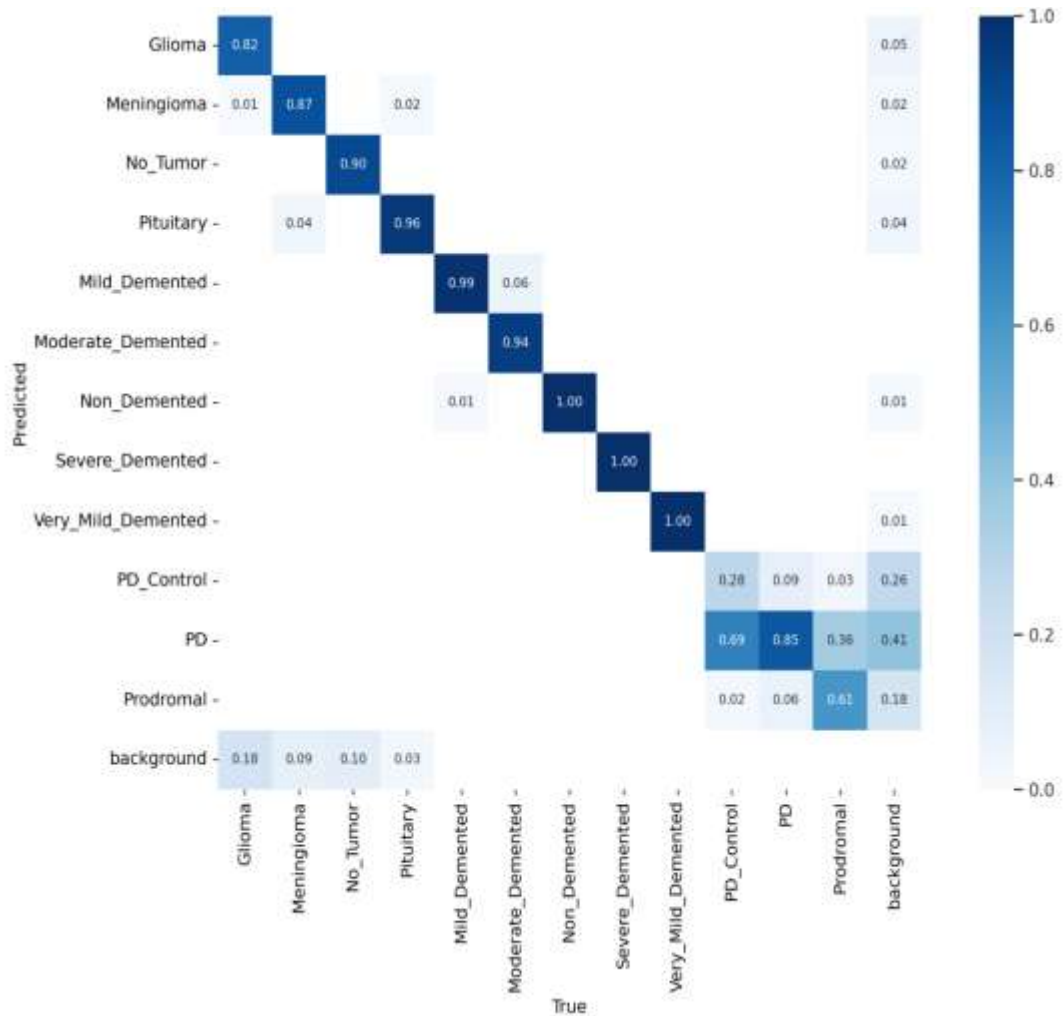


Fig. 4:- F1 vs. Confidence Curve for YOLOv10-N model.

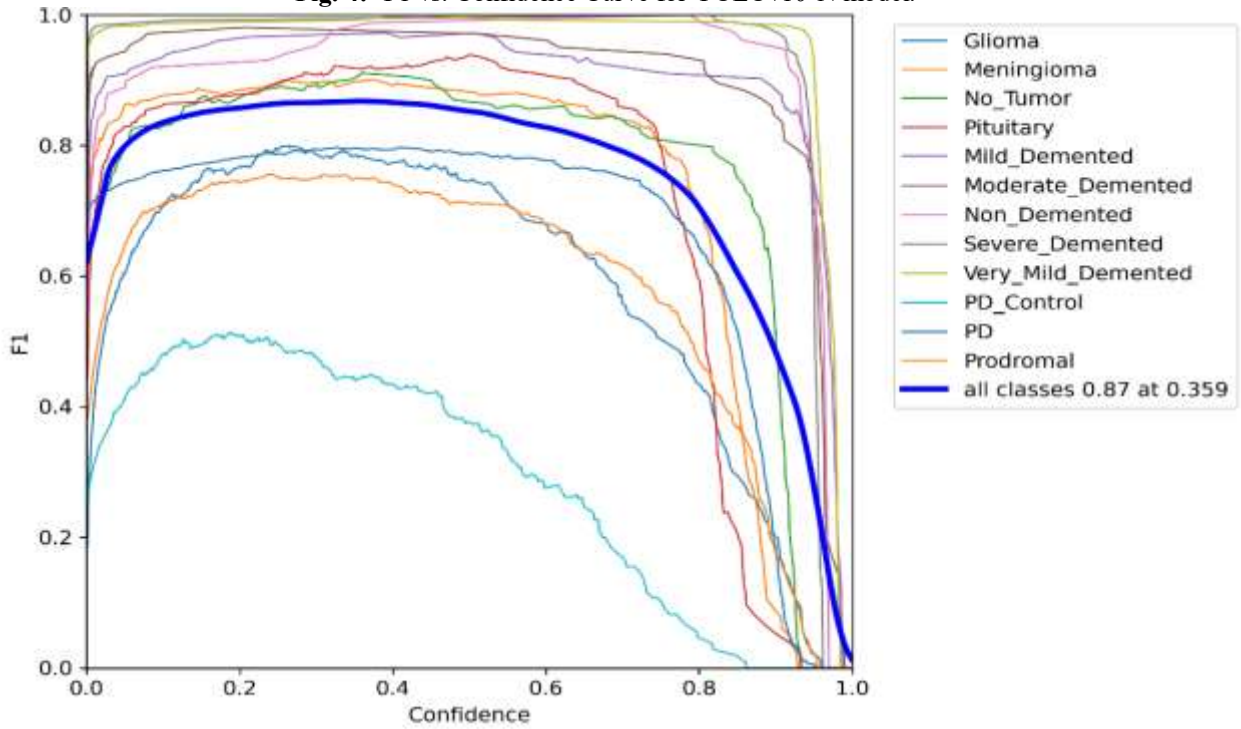


Fig. 5:- Precision vs. Recall Curve for YOLOv10-N model.

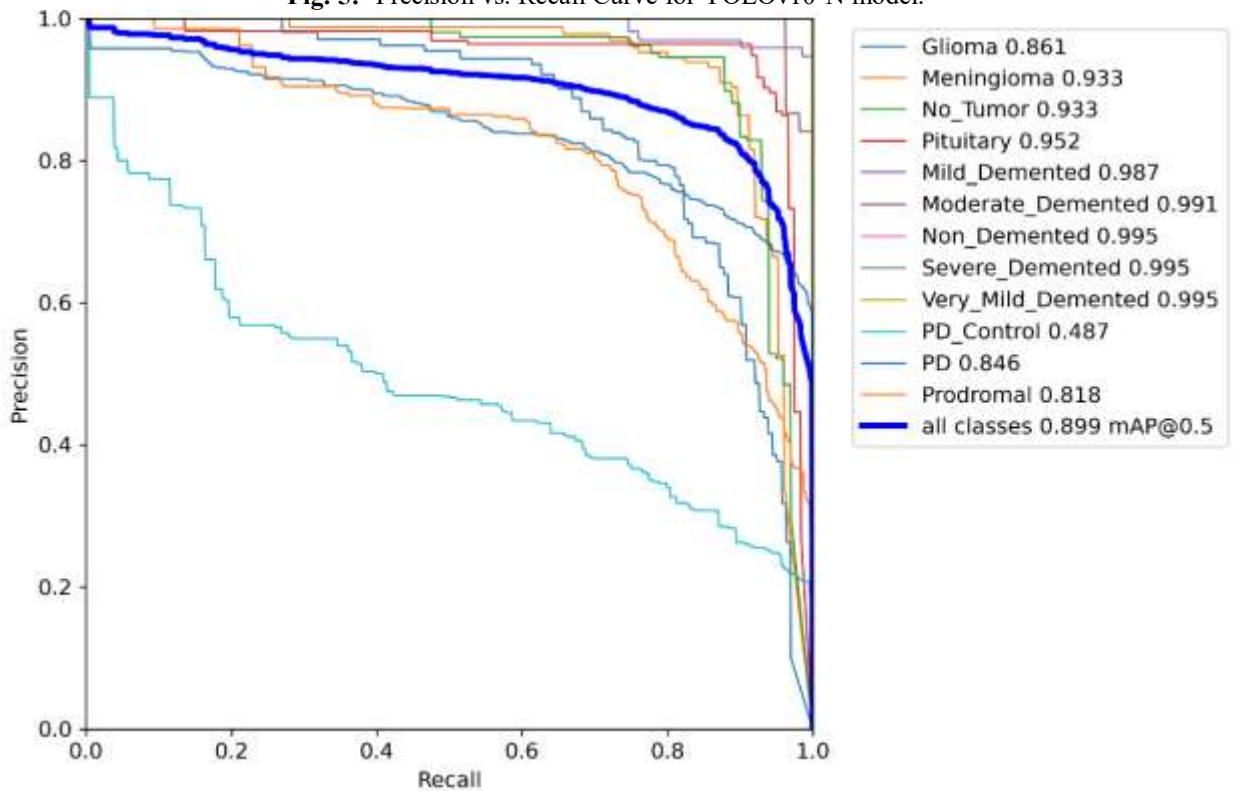
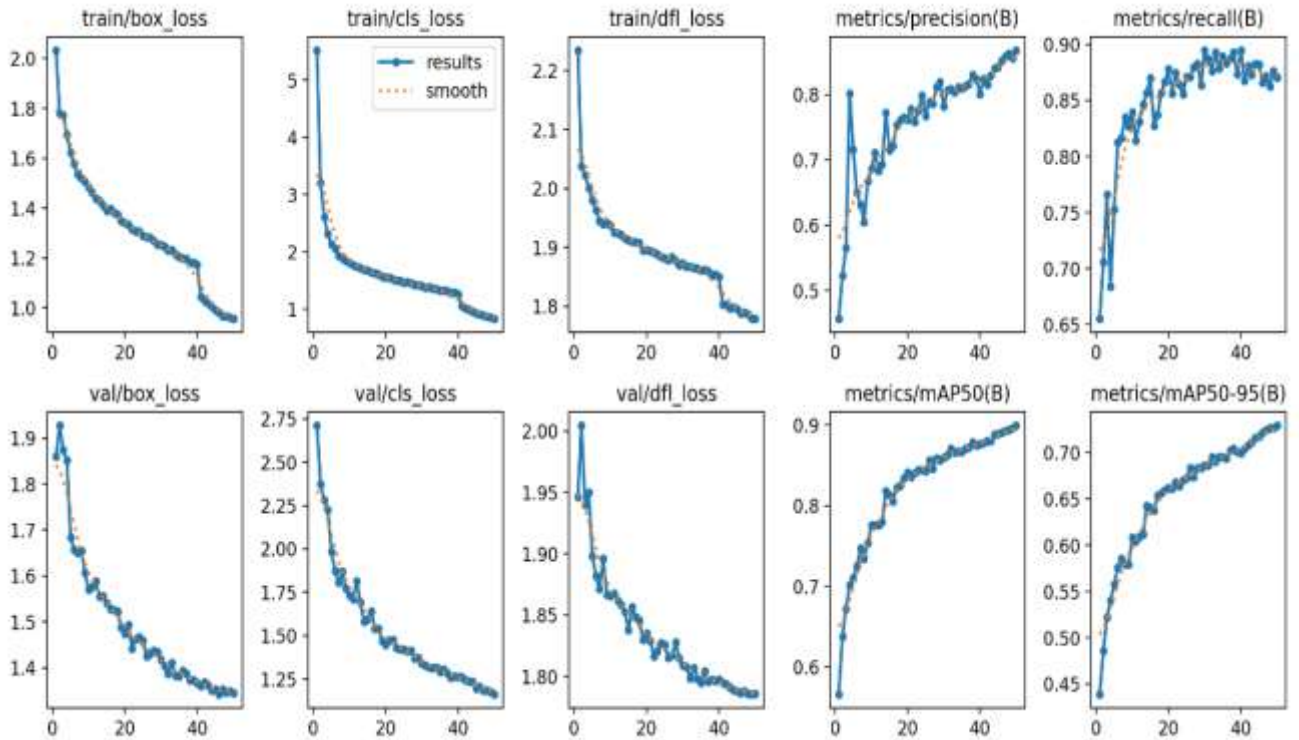


Fig. 6:- Graphical Representation of Performance Analysis for YOLOv10-N model.



YOLOv10-S Model

The YOLOv10-S model, containing 8.08 million parameters, demonstrated improved recall at 90.4% and slightly lower precision at 86.32%. Its F1-Score was 88.31%, with mAP50 reaching 91.81% and mAP50–95 at 75.89%. The average latency per image was similar to YOLOv10-N at 25.08 milliseconds, offering a balanced trade-off between accuracy and efficiency.

Table 5:- Performance Analysis for YOLOv10-S model.

Model	Image Size	Epochs	Total No. Parameters	FLOPs (G)	Precision (%)	Recall (%)	F1-Score (%)	mAP 50 (Val) (%)	mAP 50-95 (Val) (%)	Avg. Latency (Val) (ms)
YOLOv10-S	320	50	8.08 M (8,075,640)	24.8	86.32	90.40	88.31	91.81	75.89	25.08

Fig. 7:- Confusion Matrix (Normalized) for YOLOv10-S model.

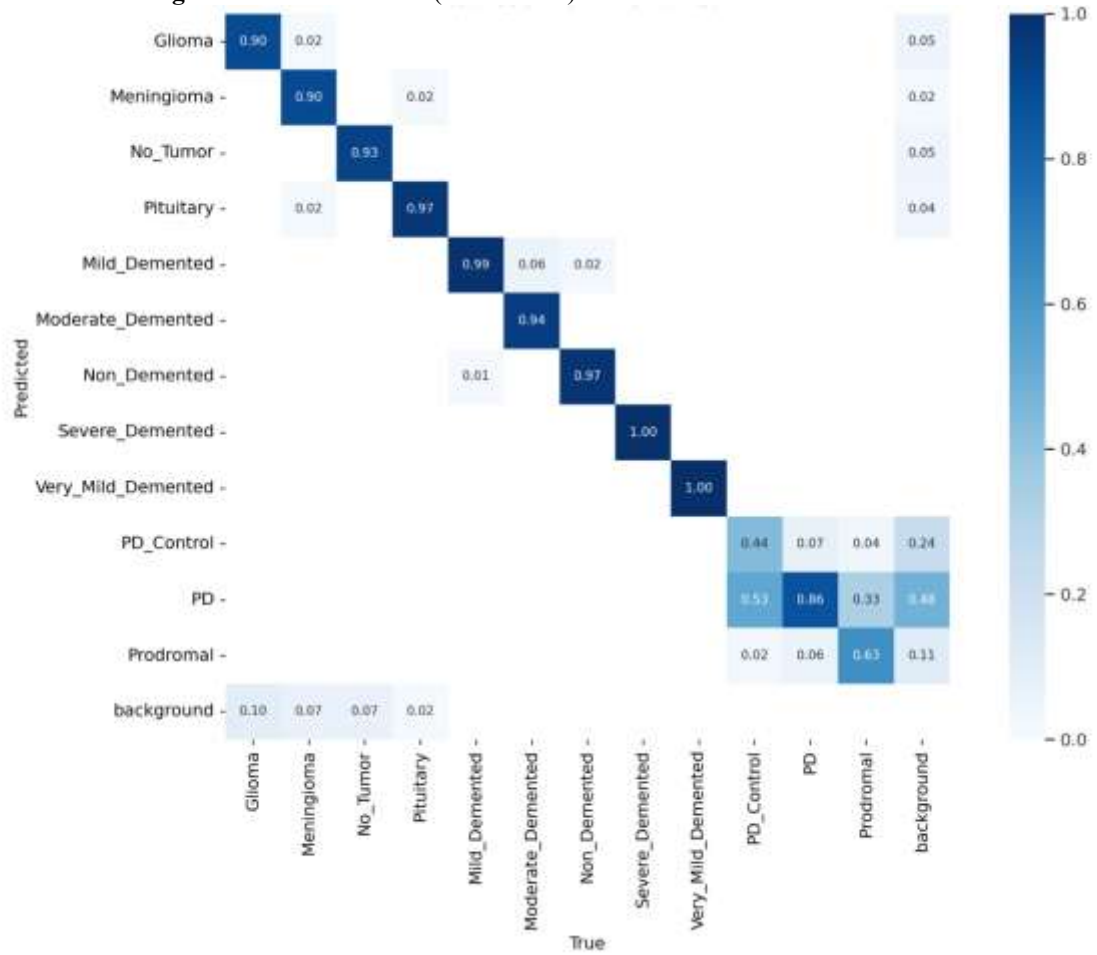


Fig. 8:- F1 vs. Confidence Curve for YOLOv10-S model.

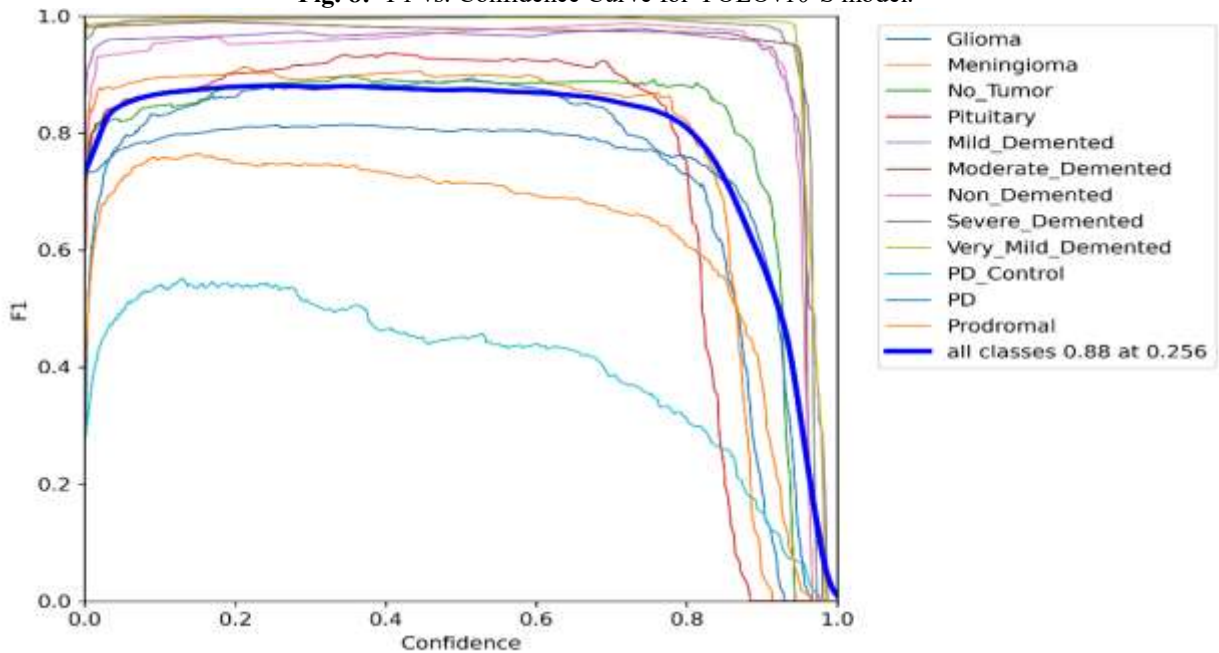


Fig. 9:- Precision vs. Recall Curve for YOLOv10-S model.

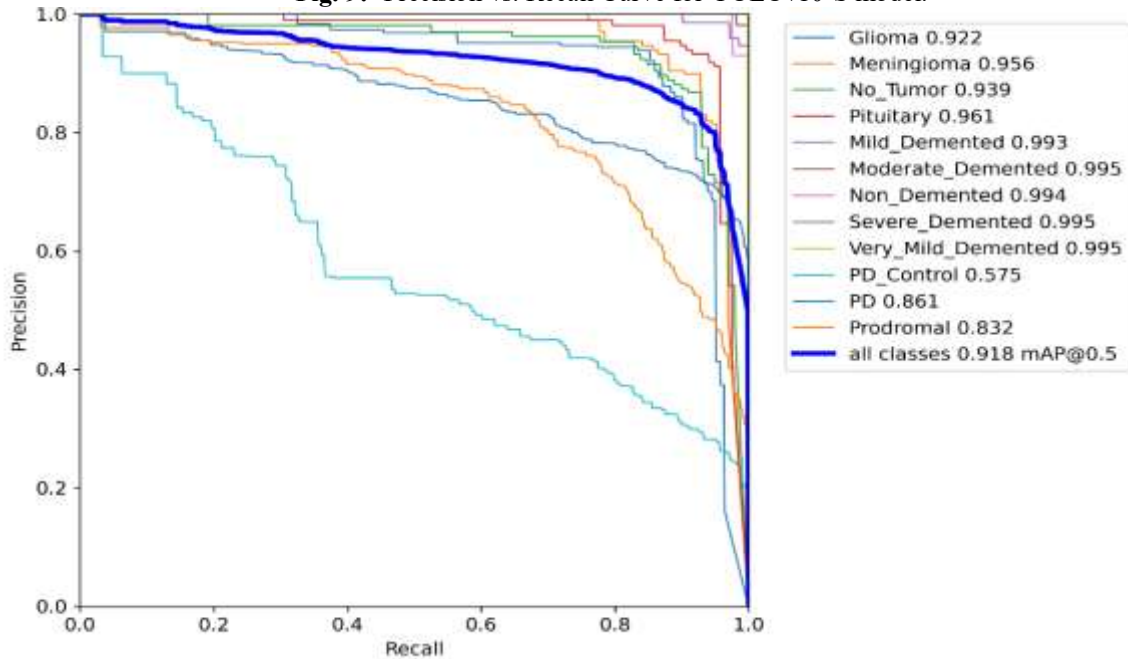
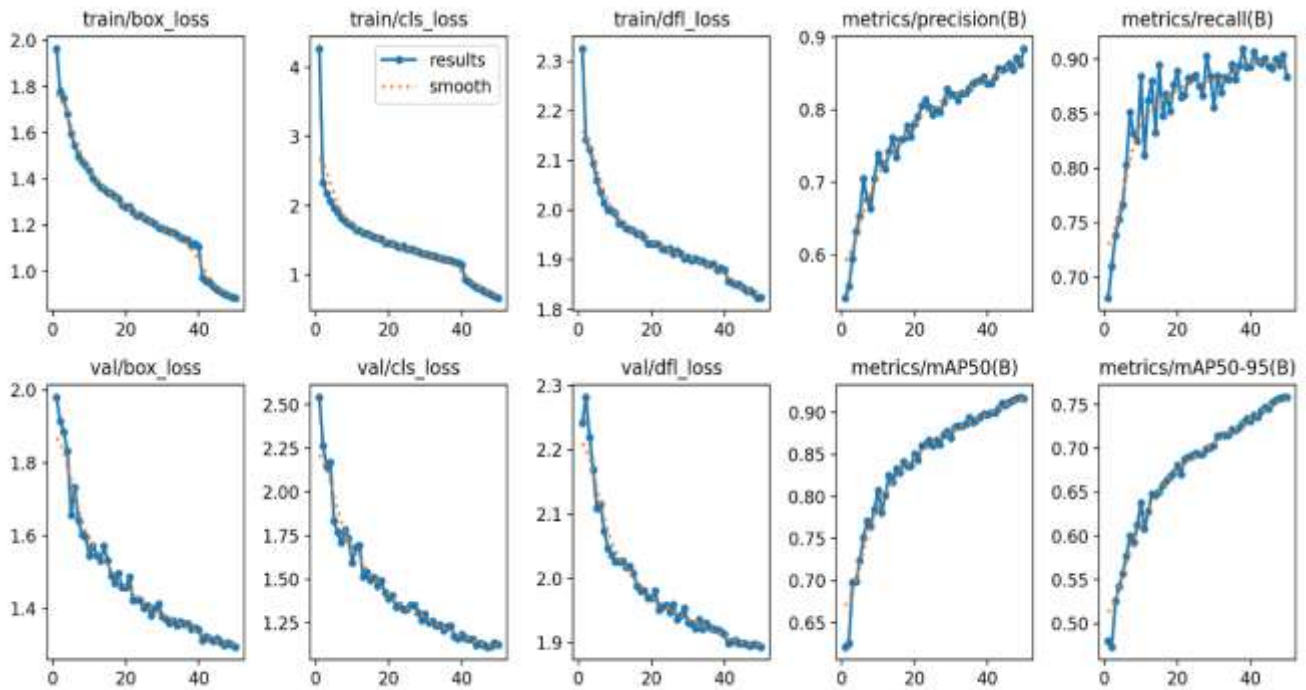


Fig. 10:- Graphical Representation of Performance Analysis for YOLOv10-S model.



YOLOv10-M Model:

The YOLOv10-M model, comprising 16.50 million parameters, achieved a high precision of 90.08% but slightly reduced recall at 86.66%. Its F1-Score stood at 88.34%, with a mAP50 of 91.63% and mAP50-95 at 75.45%. The model exhibited an average latency of 27.67 milliseconds, indicating its suitability for applications requiring moderate computational power.

Table 6:- Performance Analysis for YOLOv10-M model.

Model	Image Size	Epochs	Total No. Parameters	FLOPs (G)	Precision (%)	Recall (%)	F1-Score (%)	mAP 50 (Val) (%)	mAP 50-95 (Val) (%)	Avg. Latency (Val) (ms)
YOLOv10-M	320	50	16.50 M (16,498,024)	64.0	90.08	86.66	88.34	91.63	75.45	27.67

Fig. 11:- Confusion Matrix (Normalized) for YOLOv10-M model.

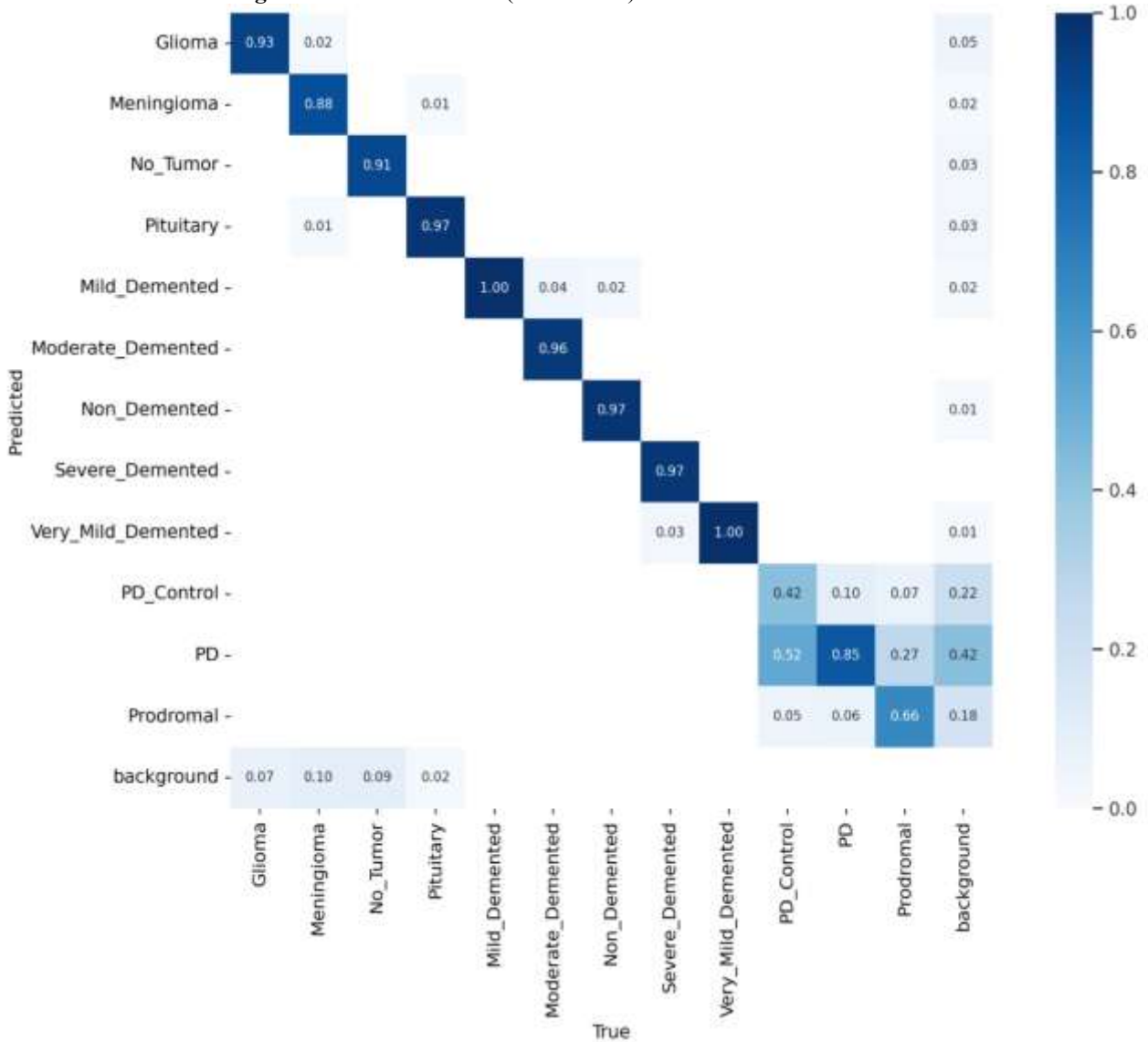


Fig. 12:- F1 vs. Confidence Curve for YOLOv10-M model.

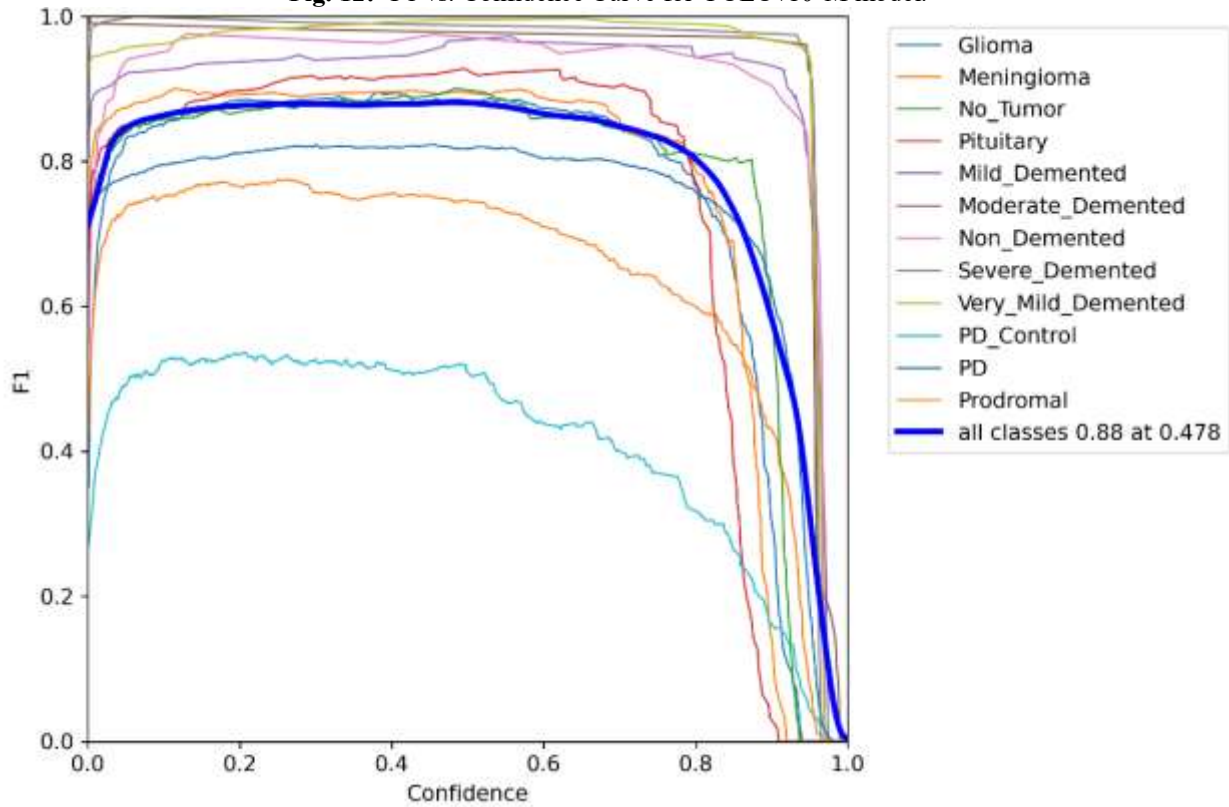


Fig. 13:- Precision vs. Recall Curve for YOLOv10-M model.

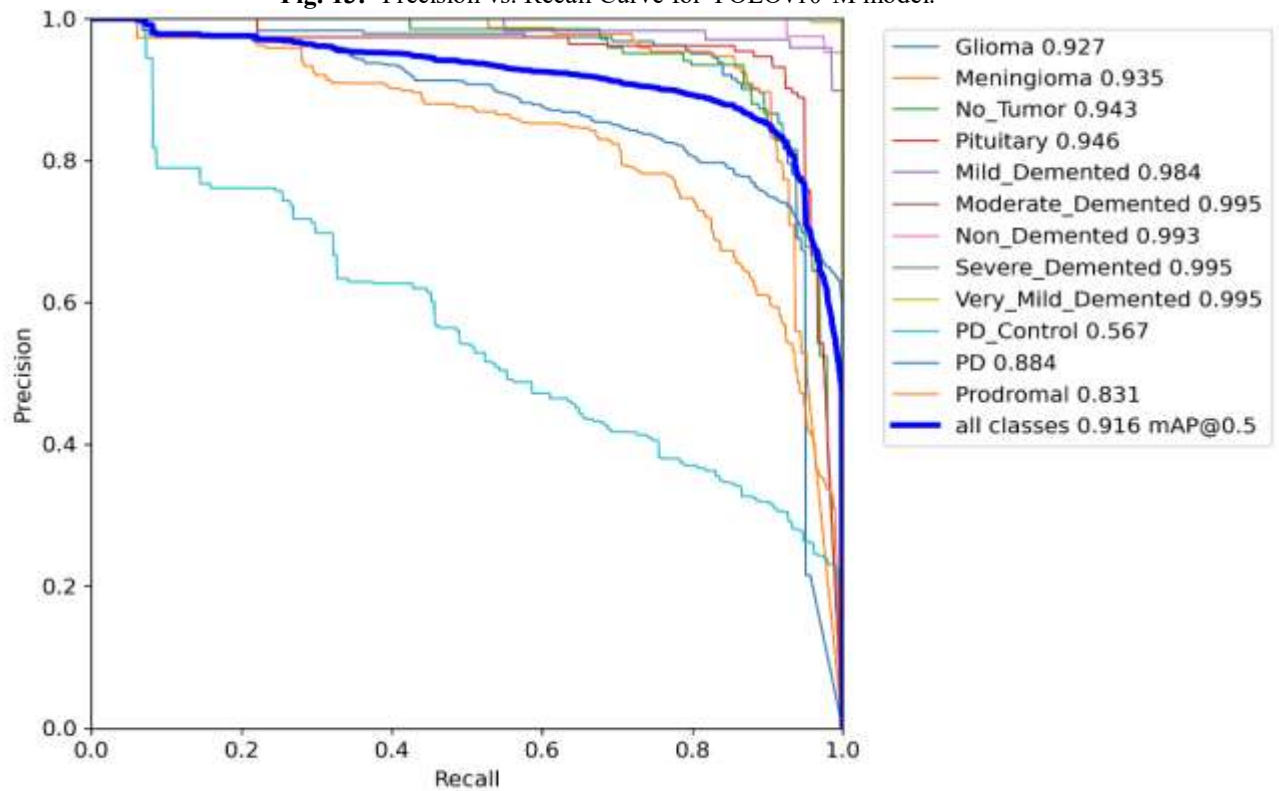
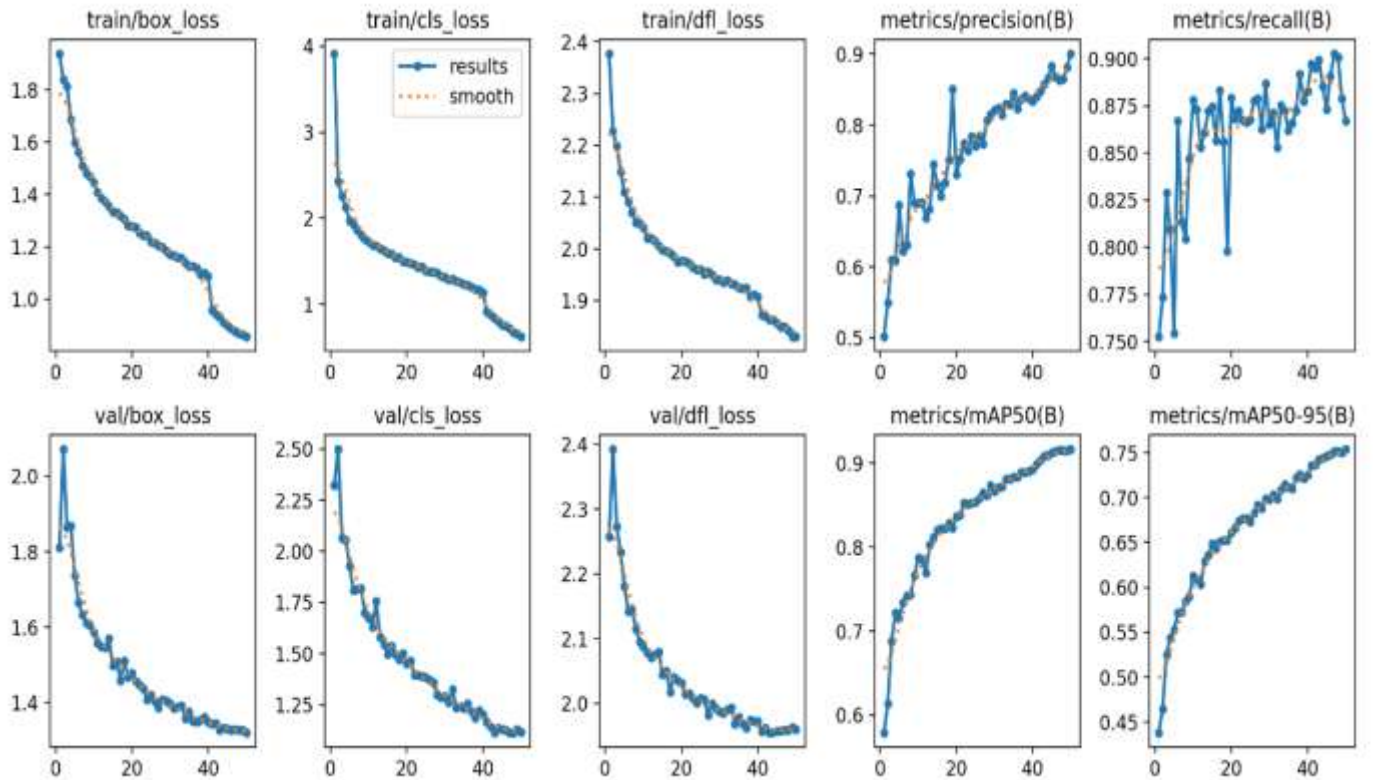


Fig. 14:- Graphical Representation of Performance Analysis for YOLOv10-M model.



YOLOv10-B Model:

The YOLOv10-B model, with 20.47 million parameters, balanced its performance with a precision of 87.52% and a recall of 89.18%. It achieved an F1-Score of 88.34%, a mAP50 of 91.71%, and a mAP50–95 of 76.09%. The latency was measured at 27.59 milliseconds, making it an efficient option for slightly larger workloads.

Table 7:- Performance Analysis for YOLOv10-B model.

Model	Image Size	Epochs	Total No. Parameters	FLOPs (G)	Precision (%)	Recall (%)	F1-Score (%)	mAP 50 (Val) (%)	mAP 50-95 (Val) (%)	Avg. Latency (Val) (ms)
YOLOv10-B	320	50	20.47 M (20,469,528)	98.8	87.52	89.18	88.34	91.71	76.09	27.59

Fig. 15:- Confusion Matrix (Normalized) for YOLOv10-B model.

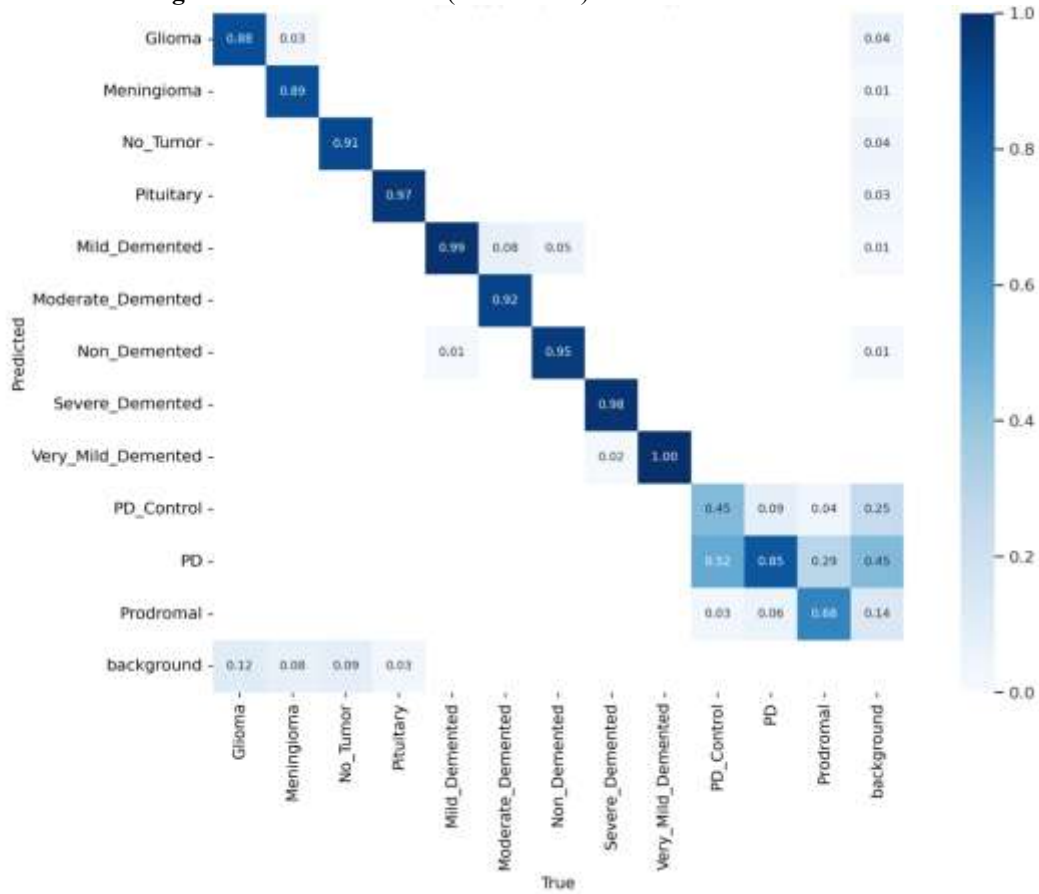


Fig. 16:- F1 vs. Confidence Curve for YOLOv10-B model.

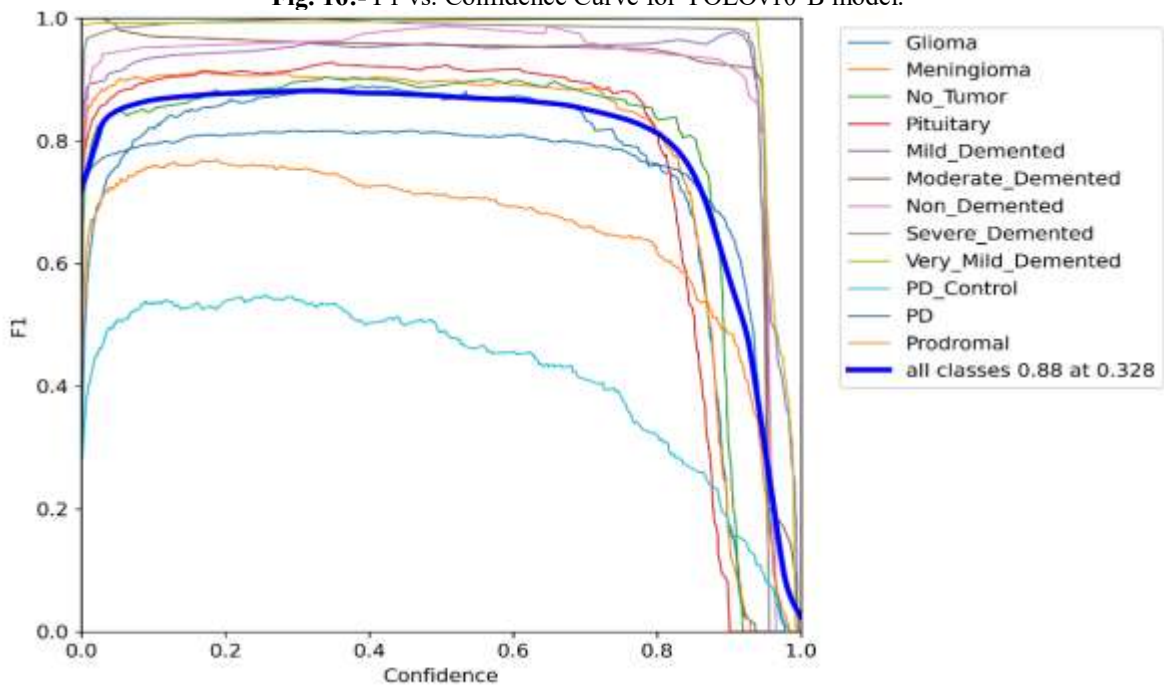


Fig. 17:- Precision vs. Recall Curve for YOLOv10-B model.

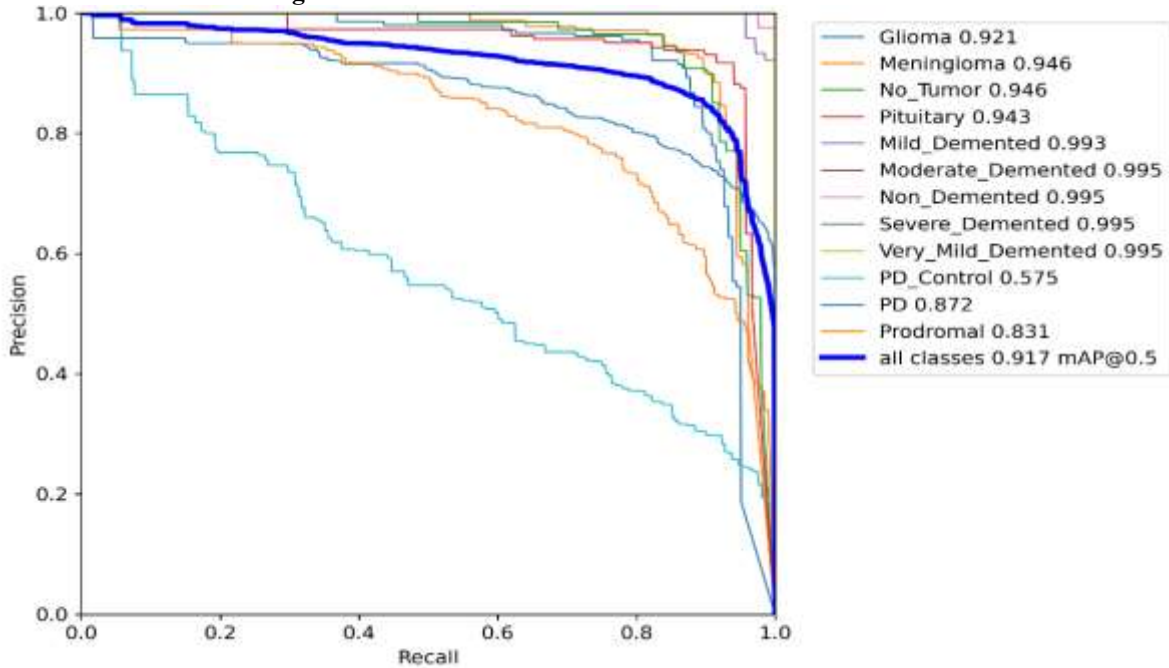
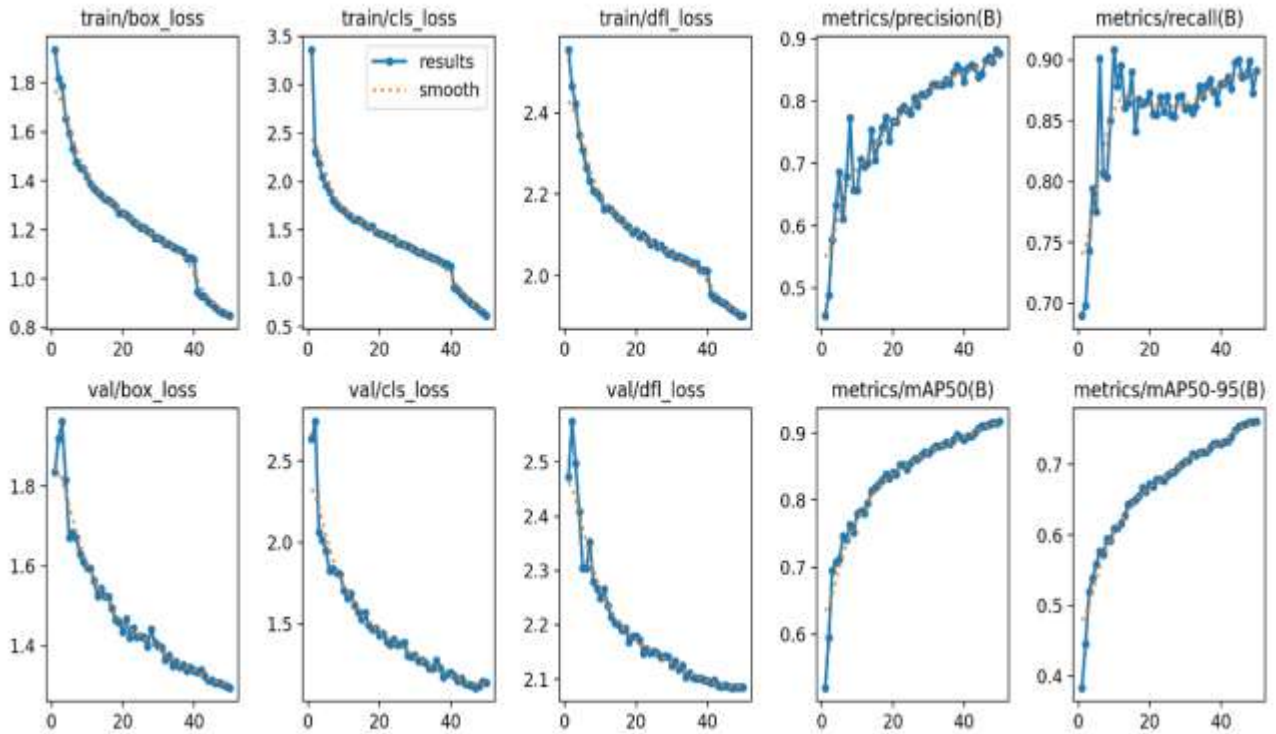


Fig. 18:- Graphical Representation of Performance Analysis for YOLOv10-B model.



YOLOv10-L Model:

The YOLOv10-L model, featuring 25.78 million parameters, exhibited precision of 87.01% and the highest recall among models at 90.84%. It delivered an F1-Score of 88.88%, a mAP50 of 92.05%, and a mAP50-95 of 76.34%. The average latency of 32.20 milliseconds reflected its computational complexity.

Table 8. Performance Analysis for YOLOv10-L model.

Model	Image Size	Epochs	Total No. Parameters	FLOPs (G)	Precision (%)	Recall (%)	F1-Score (%)	mAP 50 (Val) (%)	mAP 50-95 (Val) (%)	Avg. Latency (Val) (ms)
YOLOv10-L	320	50	25.78 M (25,783,832)	127.3	87.01	90.84	88.88	92.05	76.34	32.20

Fig. 19:- Confusion Matrix (Normalized) for YOLOv10-L model.

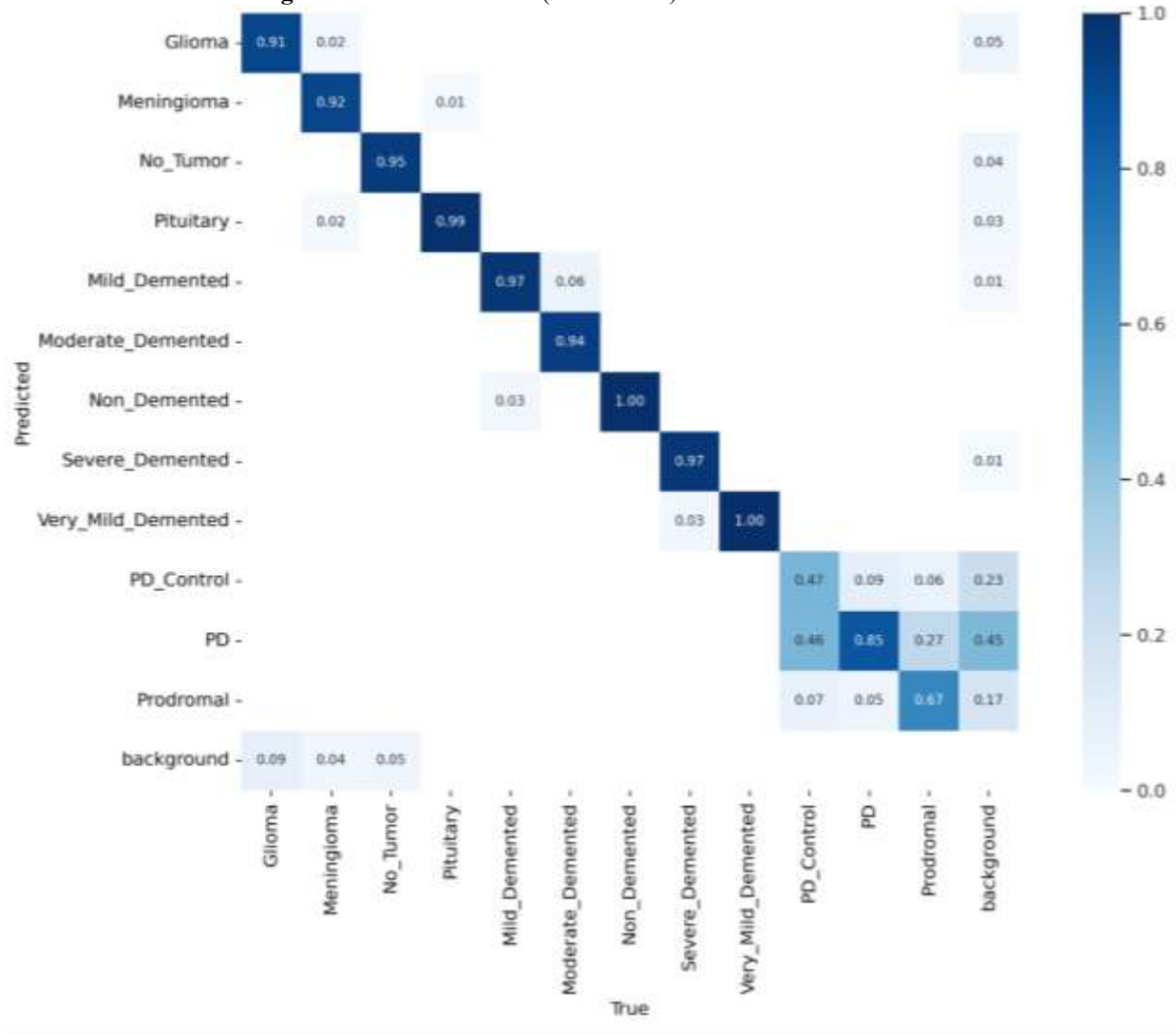


Fig. 20:-F1 vs. Confidence Curve for YOLOv10-L model.

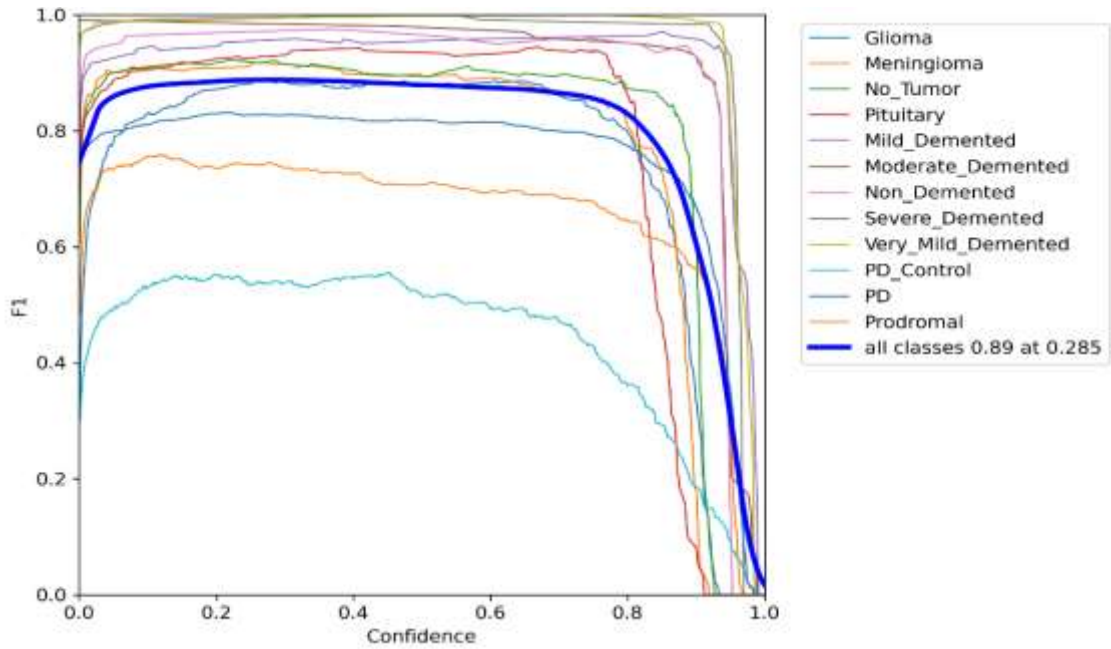


Fig. 21:- Precision vs. Recall Curve for YOLOv10-L model.

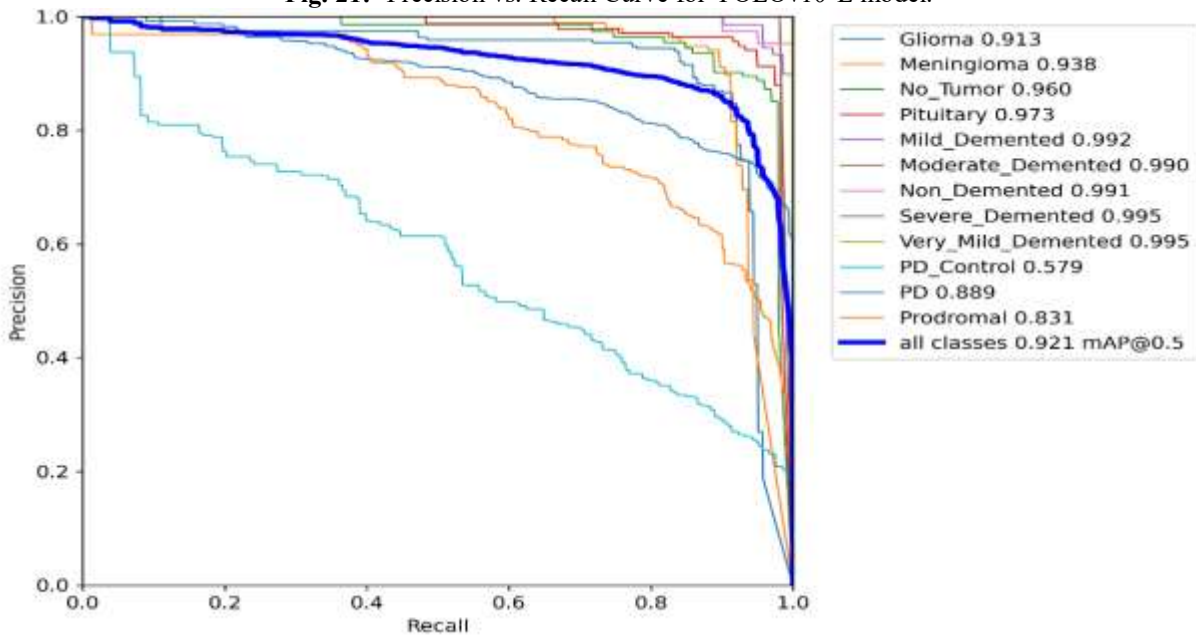
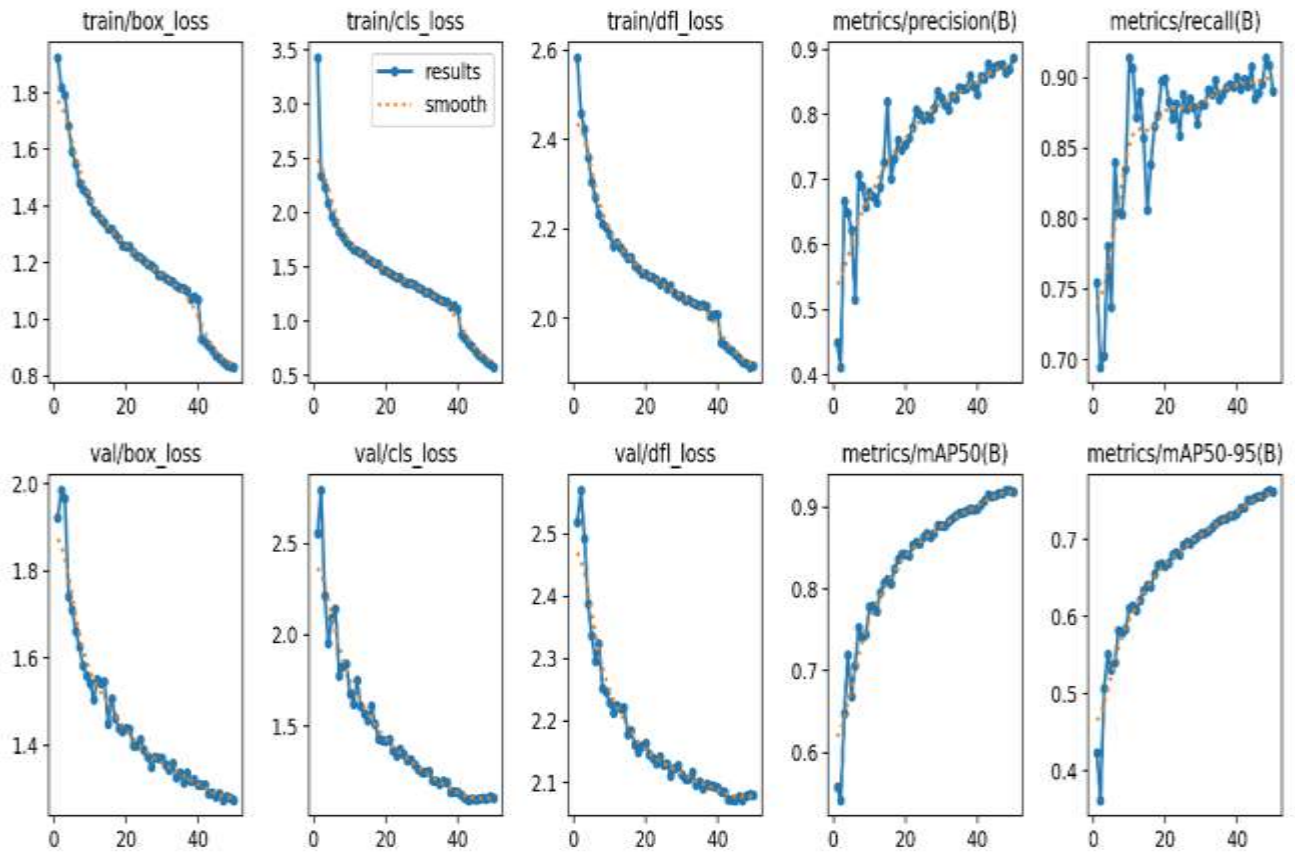


Fig. 22:- Graphical Representation of Performance Analysis for YOLOv10-L model.



YOLOv10-X Model:

The YOLOv10-X model, the largest with 31.68 million parameters, achieved the highest precision (89.94%), recall (89.02%), and F1-Score (89.48%). It also recorded the best mAP50 (92.95%) and mAP50-95 (77.31%). However, its average latency was the highest at 34.49 milliseconds, making it ideal for accuracy-critical tasks with sufficient computational resources.

Table 9:- Performance Analysis for YOLOv10-X model.

Model	Image Size	Epochs	Total No. Parameters	FLOPs (G)	Precision (%)	Recall (%)	F1-Score (%)	mAP 50 (Val) (%)	mAP 50-95 (Val) (%)	Avg. Latency (Val) (ms)
YOLOv10-X	320	50	31.68 M (31,677,992)	171.1	89.94	89.02	89.48	92.95	77.31	34.49

Fig. 23:- Confusion Matrix (Normalized) for YOLOv10-X model.

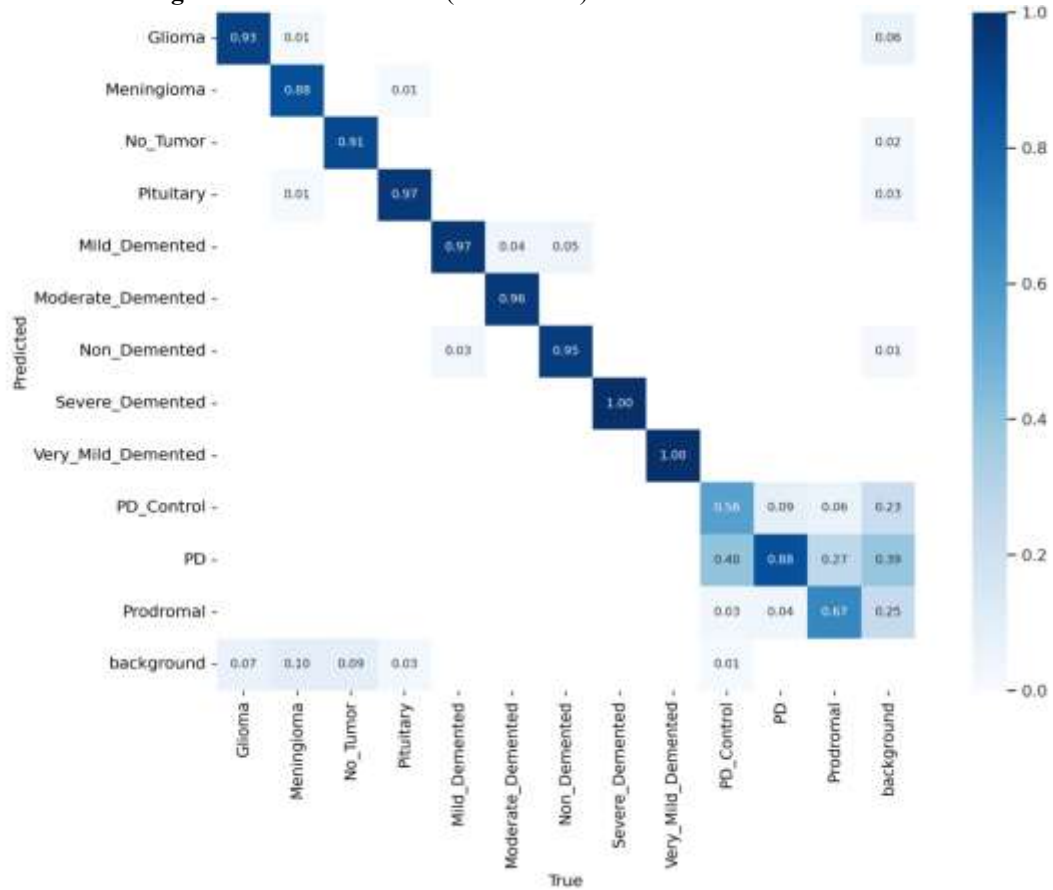


Fig. 24:- F1 vs. Confidence Curve for YOLOv10-X model.

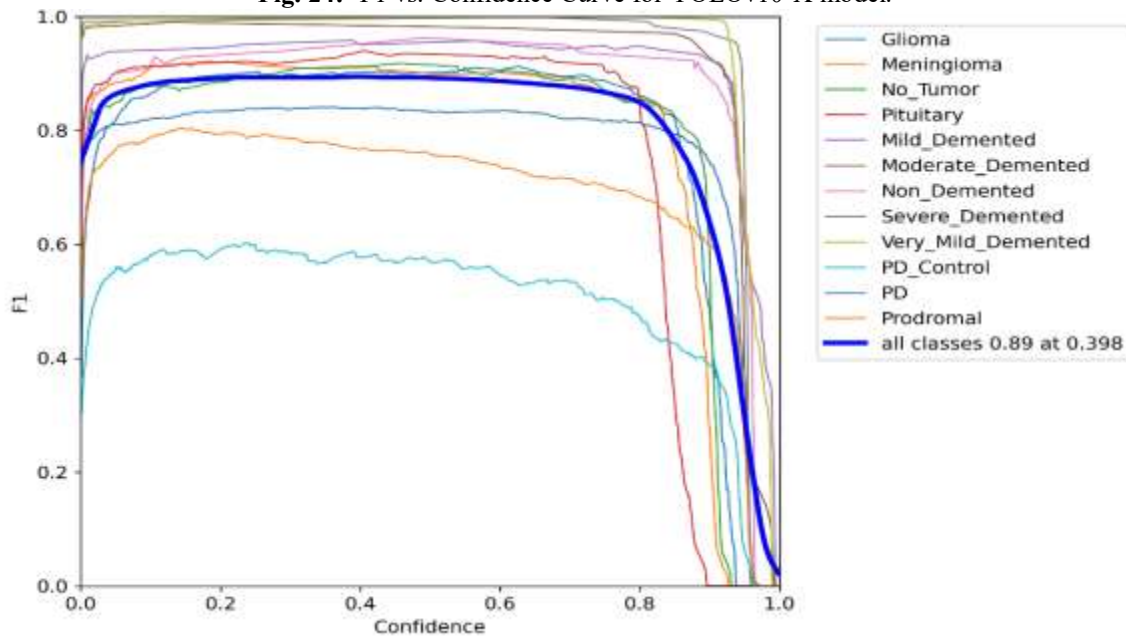


Fig. 25:- Precision vs. Recall Curve for YOLOv10-X model.

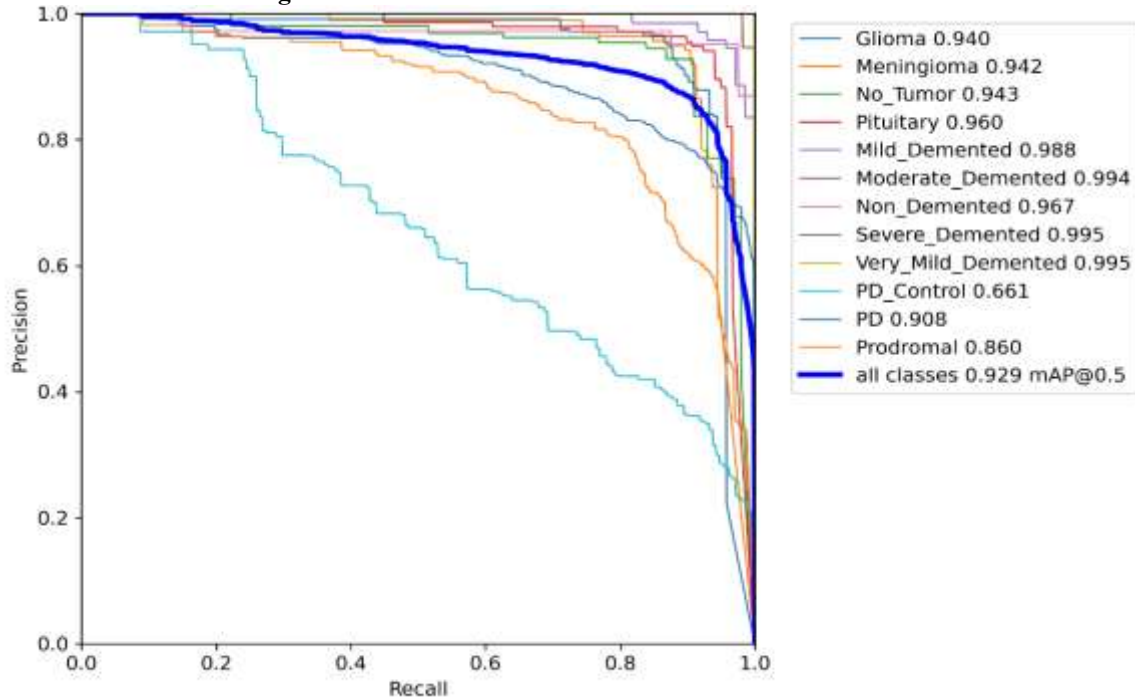
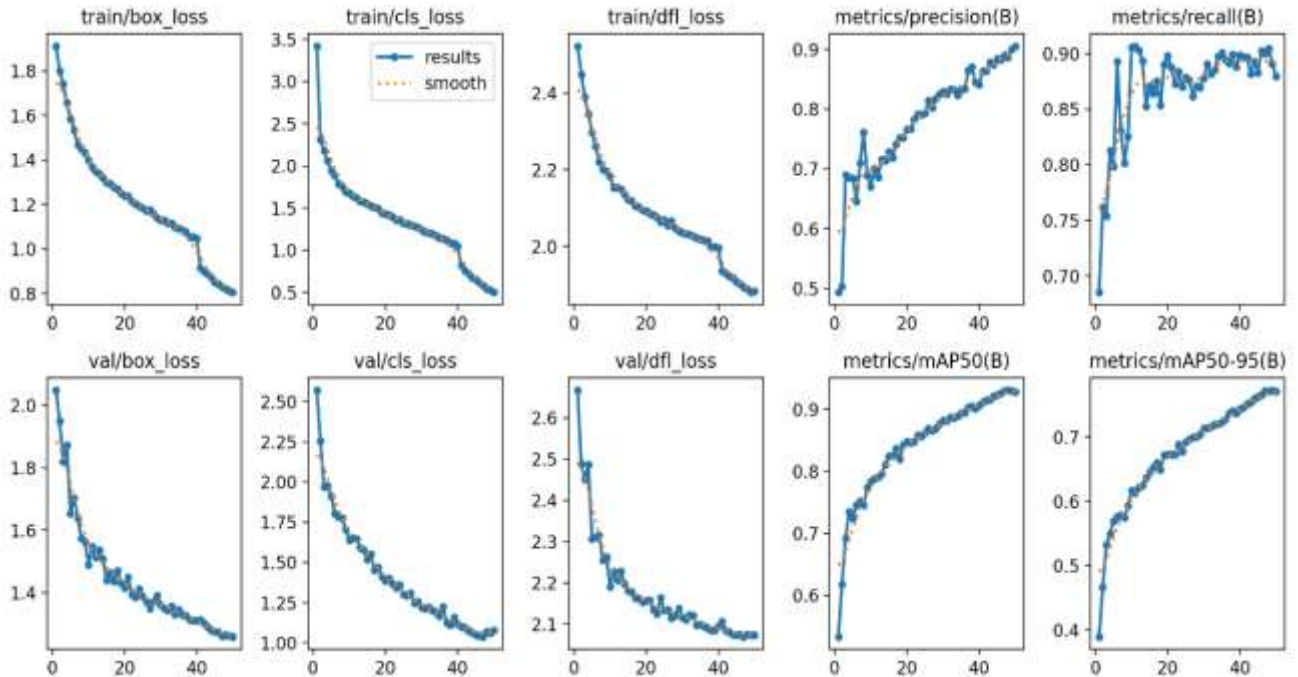


Fig. 26:- Graphical Representation of Performance Analysis for YOLOv10-X model.



Comparative Performance Analysis of YOLOv10 Models for Neurological Disease Diagnosis

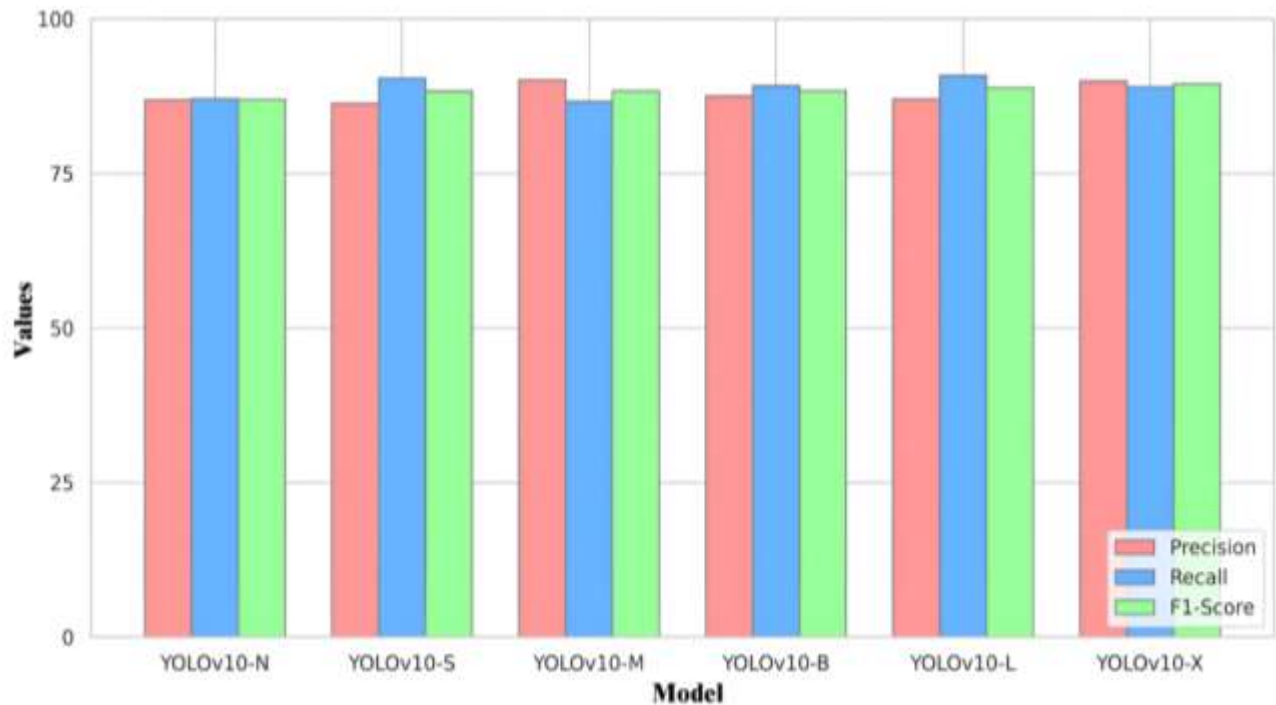
The YOLOv10 models demonstrate varying performance levels in diagnosing neurological diseases from MRI images, depending on their complexity. YOLOv10-X achieves the highest diagnostic accuracy, with precision (89.94%), recall (89.02%), and F1-score (89.48%), making it the most effective for detecting and localizing abnormalities such as gliomas, meningiomas, and pituitary tumors. The lighter models, YOLOv10-N and YOLOv10-S, still provide reliable results with an mAP@50 of 89.94% and 91.81%, respectively, while maintaining

significantly lower computational demands. These models are particularly suitable for real-time diagnostic workflows in resource-constrained clinical settings, offering a balance of performance and efficiency [79-81].

Table 10:- An overview of evaluation results and Performance Analysis for all YOLOv10 Models used in Proposed Work.

Model	Image Size	Epochs	Total No. Parameters	FLOPs (G)	Precision (%)	Recall (%)	F1-Score (%)	mAP 50 (Val) (%)	mAP 50-95 (Val) (%)	Avg. Latency (Val) (ms)
YOLOv10-N	320	50	2.71 M (2,711,720)	8.4	86.89	87.07	86.98	89.94	72.98	25.10
YOLOv10-S	320	50	8.08 M (8,075,640)	24.8	86.32	90.40	88.31	91.81	75.89	25.08
YOLOv10-M	320	50	16.50 M (16,498,024)	64.0	90.08	86.66	88.34	91.63	75.45	27.67
YOLOv10-B	320	50	20.47 M (20,469,528)	98.8	87.52	89.18	88.34	91.71	76.09	27.59
YOLOv10-L	320	50	25.78 M (25,783,832)	127.3	87.01	90.84	88.88	92.05	76.34	32.20
YOLOv10-X	320	50	31.68 M (31,677,992)	171.1	89.94	89.02	89.48	92.95	77.31	34.49

Fig. 27:- Graphical Representation of Comparison of Precision, Recall, and F1-Score for all YOLOv10 models.



Performance Efficiency Trade-Off Analysis of YOLOv10 Models in Medical Diagnostics

In the context of medical image analysis for neurological diseases, the performance-efficiency trade-off of YOLOv10 models is critical. Lighter models, such as YOLOv10-N and YOLOv10-S, exhibit low latency (25.10 ms and 25.08 ms, respectively), enabling faster diagnostic decisions while maintaining moderate accuracy, making them ideal for rapid screening in emergency or mobile healthcare units. On the other hand, YOLOv10-X, with its higher computational complexity and latency (34.49 ms), provides the most accurate segmentation and localization of

disease-specific regions in MRI images, suitable for detailed diagnostic analysis and treatment planning in specialized healthcare centers. This trade-off underscores the importance of selecting the appropriate model based on the diagnostic requirements and available computational resources [1,82,83].

Fig. 28:- Graphical Representation of FLOPs (G) vs. mAP50 for all YOLOv10 models.

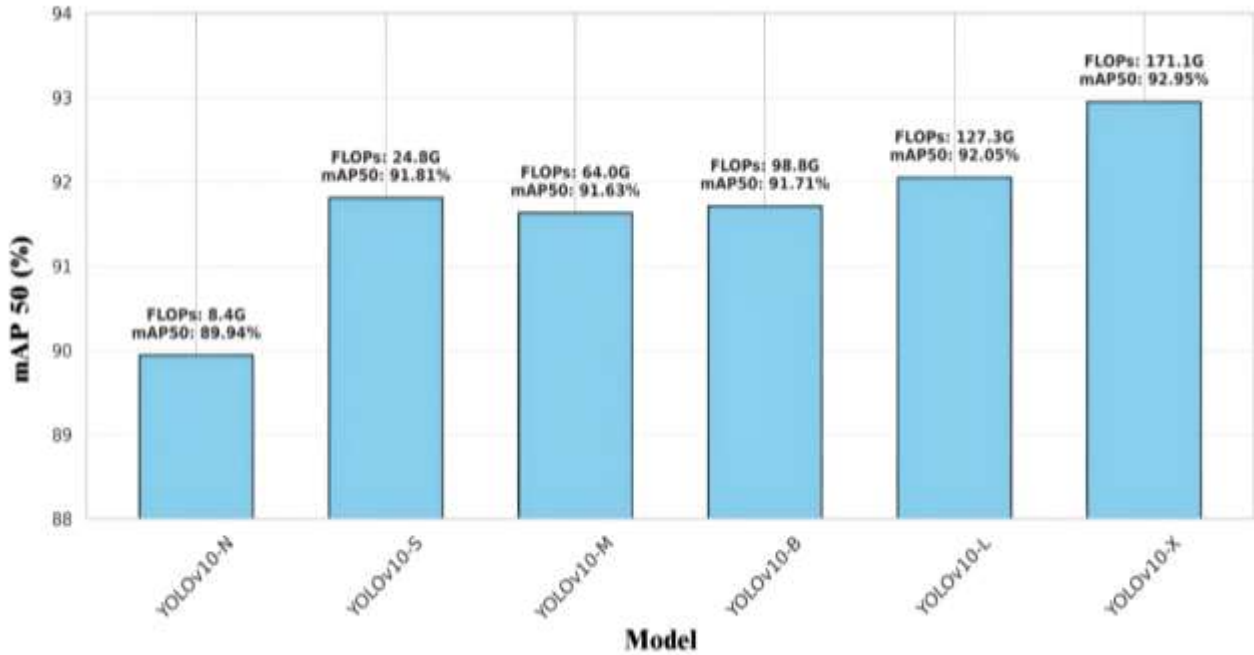
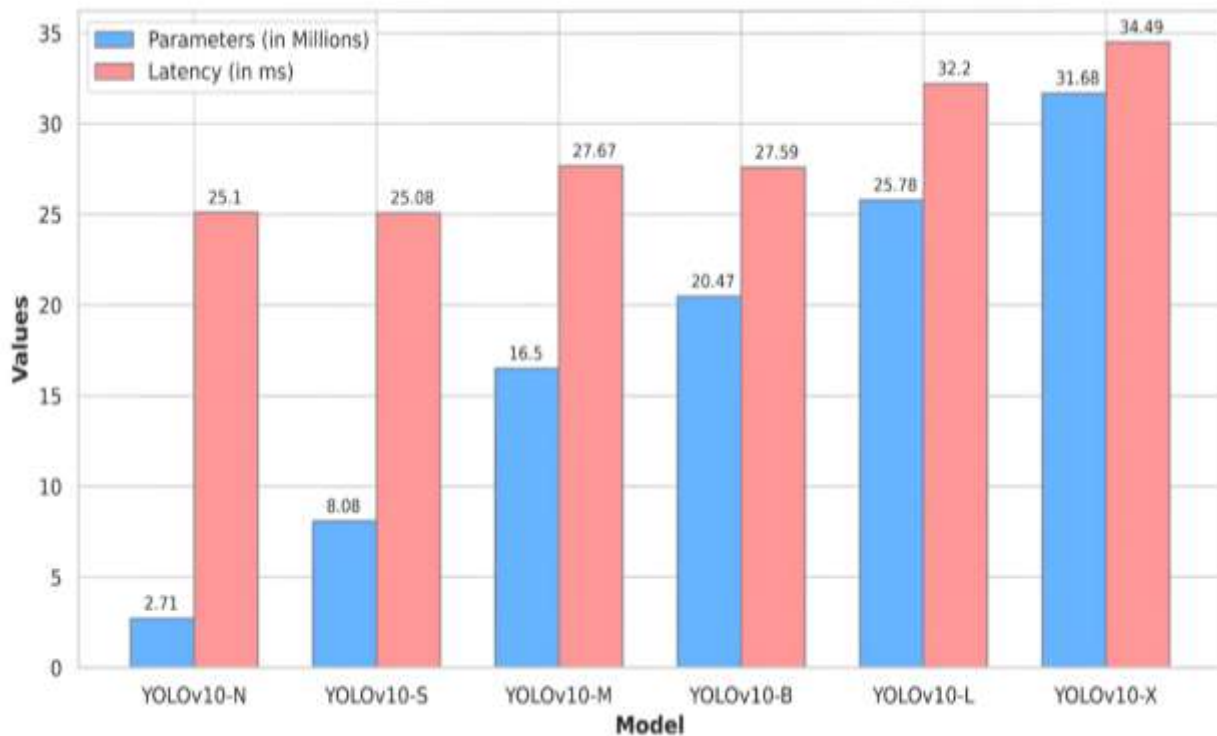


Fig. 29:- Graphical Representation of Parameter (in Millions) vs. Latency (in ms) for all YOLOv10 models.



Segmentation and Interpretation

1. **Input Image:** Raw MRI images from various classes are used as the primary input for analysis. These images undergo preprocessing to prepare them for detection and segmentation tasks [75].
2. **Bounding Box Detection:** The YOLOv10-X model detects regions of interest by generating bounding boxes around potential abnormalities or class-specific features. Its high performance ensures precise localization, making it suitable for complex medical imaging tasks [76].
3. **Detection Details:** Each bounding box includes a class label and a confidence score, which aids in the accurate prediction and localization of the detected region. These details are crucial for validating the reliability of the model's predictions [76].
4. **SAM 2.1 Output:** The "Segment Anything Model (SAM) 2.1-tiny" refines the detection process by creating segmentation masks for the bounding boxes. These masks enhance the precision of the detected regions by outlining the exact areas of abnormalities or class-specific features [77].
5. **Colormap Visualization (Plasma):** The segmented regions are visualized using a Plasma Colormap. This step highlights activated areas, providing an interpretable representation of the model's predictions for better understanding in medical diagnostics [78].

Fig. 30:- Segmentation and Interpretation for Brain Tumor Classes.

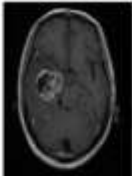
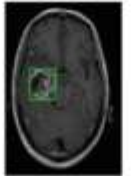
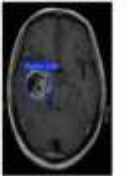
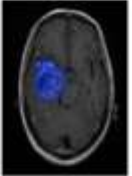
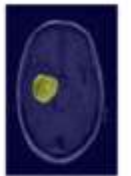
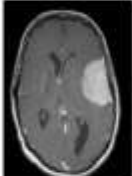
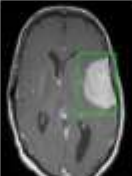
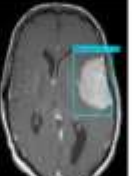
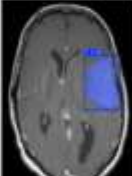
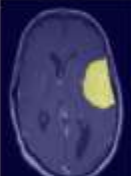



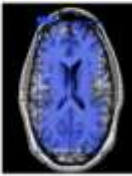

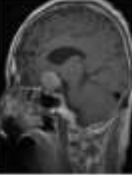
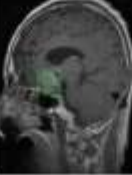

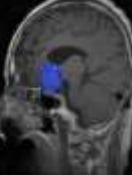
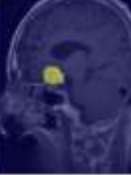
Index	Class	Input Image	Bounding Box	Detection	SAM 2.1 Output	Colormap Visualization (Plasma)
0	Glioma					
1	Meningioma					
2	No Tumor					
3	Pituitary					

Fig. 31:- Segmentation and Interpretation for Alzheimer’s Disease Classes.

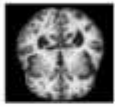

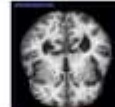
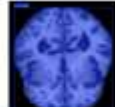

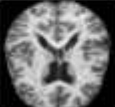


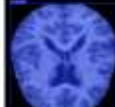
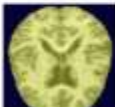
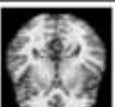

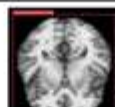
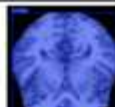


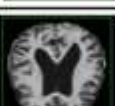

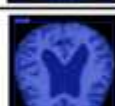

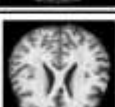


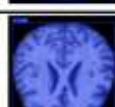

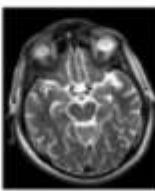
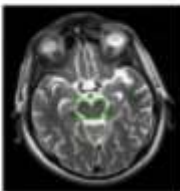
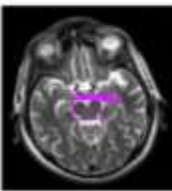
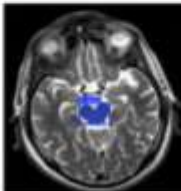
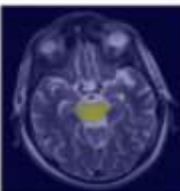

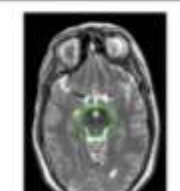
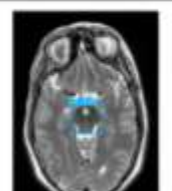
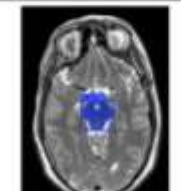
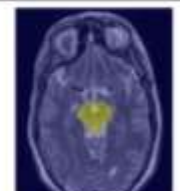
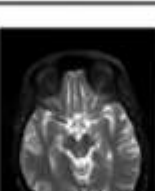
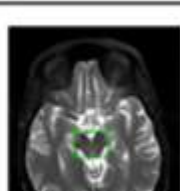
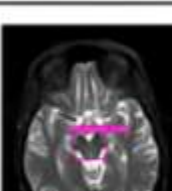
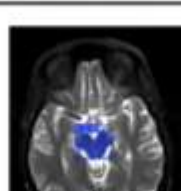
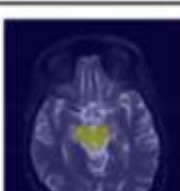
Index	Class	Input Image	Bounding Box	Detection	SAM 2.1 Output	Colormap Visualization (Plasma)
4	Mild Demented					
5	Moderate Demented					
6	No Demented					
7	Severe Demented					
8	Very Mild Demented					

Fig. 32:- Segmentation and Interpretation for Parkinson’s Disease Classes.

Index	Class	Input Image	Bounding Box	Detection	SAM 2.1 Output	Colormap Visualization (Plasma)
9	PD Control					
10	PD					
11	Prodromal					

Conclusion and Future Scope:-

This research highlights the potential of deep learning models, specifically YOLOv10 variants, in the automated detection and classification of neurological diseases from MRI images. By leveraging the strengths of YOLOv10-X for high accuracy and lighter models such as YOLOv10-N and YOLOv10-S for efficiency, the study establishes a trade-off between performance and computational requirements. The integration of advanced segmentation techniques, such as the SAM 2.1 model, further enhances the interpretability of the detected regions, which is critical for medical diagnostics. The use of colormap visualizations like Plasma further aids in the clinical understanding of disease-specific regions, making these methods practical for real-world medical applications.

Future research will focus on expanding this work by integrating multimodal medical imaging data, including CT and PET scans, to develop a more comprehensive diagnostic framework. Furthermore, incorporating explainable AI techniques such as SHAP and LIME can enhance model transparency, fostering greater trust among healthcare professionals. Another key direction involves optimizing these models for real-time deployment on edge devices, enabling deep learning-based diagnostics in resource-constrained clinical settings. These advancements aim to improve the scalability, robustness, and accessibility of AI-driven medical diagnostics, ultimately supporting healthcare practitioners in delivering precise and timely patient care.

References:-

- [1] Litjens, G., Kooi, T., Bejnordi, B.E., Setio, A.A.A., Ciompi, F., Ghafoorian, M., van der Laak, J.A.W.M., van Ginneken, B., Sánchez, C.I.: A Survey on Deep Learning in Medical Image Analysis. *Med. Image Anal.* 42, 60-88 (2017). <https://doi.org/10.1016/j.media.2017.07.005>
- [2] Esteva, A., Robicquet, A., Ramsundar, B., Kuleshov, V., DePristo, M., Chou, K., Cui, C., Corrado, G.S., Thrun, S., Dean, J.: Deep Learning-enabled Medical Computer Vision. *Nat. Biomed. Eng.* 5, 635-646 (2021). <https://doi.org/10.1038/s41551-020-00640-y>
- [3] Bochkovskiy, A., Wang, C.Y., Liao, H.Y.M.: YOLOv4: Optimal Speed and Accuracy of Object Detection. arXiv preprint arXiv:2004.10934 (2020). <https://arxiv.org/abs/2004.10934>
- [4] A. Kirillov et al., "Segment anything," in Proceedings of the IEEE/CVF International Conference on Computer Vision, pp. 4015-4026, 2023.
- [5] M. L. Giger, "Machine Learning in Medical Imaging," *Journal of the American College of Radiology*, vol. 15, no. 3, pt. B, pp. 512-520, 2018. doi: 10.1016/j.jacr.2017.12.028.
- [6] A. Nanda, R. C. Barik, and S. Bakshi, "SSO-RBNN driven brain tumor classification with Saliency-K-means segmentation technique," *Biomedical Signal Processing and Control*, vol. 81, p. 104356, 2023. doi: 10.1016/j.bspc.2022.104356.
- [7] Saboor, A., Li, J. P., Haq, A. U., Shehzad, U., Khan, S., Aotaibi, R. M., & Alajlan, S. A. (2024). DDFC: deep learning approach for deep feature extraction and classification of brain tumors using magnetic resonance imaging in E-healthcare system. *Scientific Reports*, 14, 6425. <https://doi.org/10.1038/s41598-024-56983-6>
- [8] S. Srinivasan et al., "A hybrid deep CNN model for brain tumor image multi-classification," *BMC Medical Imaging*, 2024. [Online]. Available: <https://doi.org/10.1186/s12880-024-01195-7>.
- [9] Roy, P., Srijon, F. M. S., & Bhowmik, P. (2024). An explainable ensemble approach for advanced brain tumor classification applying Dual-GAN mechanism and feature extraction techniques over highly imbalanced data. *PLOS ONE*, 19(9), e0310748. <https://doi.org/10.1371/journal.pone.0310748>
- [10] Khalighi, S., Reddy, K., Midya, A., Pandav, K. B., Madabhushi, A., & Abedalthagafi, M. (2024). Artificial intelligence in neuro-oncology: advances and challenges in brain tumor diagnosis, prognosis, and precision treatment. *npj Precision Oncology*, 8, 80. <https://doi.org/10.1038/s41698-024-00575-0>
- [11] Almufareh, M. F., Imran, M., Khan, A., Humayun, M., & Asim, M. (2024). Automated Brain Tumor Segmentation and Classification in MRI Using YOLO-Based Deep Learning. *IEEE Access*, 12, 16189-16207. <https://doi.org/10.1109/ACCESS.2024.3359418>
- [12] Sarada, B., Reddy, K. N., Singh, M., Babu, R., & Babu, B. R. (2024). Brain Tumor Classification Using Modified ResNet50V2 Deep Learning Model. *International Journal of Computing and Digital Systems*.
- [13] Ashafuddula, N. I. Md., & Islam, R. (2024). ContourTL-Net: Contour-Based Transfer Learning Algorithm for Early-Stage Brain Tumor Detection. *International Journal of Biomedical Imaging*, 2024, Article ID 6347920. <https://doi.org/10.1155/2024/6347920>
- [14] Rajeswari, R., Sahu, S., Tripathy, R., & Sesha Sai, M. S. (2024). DFMN: Dense fused Maxout network for severity prediction of brain tumor using hybrid tumor segmentation algorithm. *Biomedical Signal Processing and Control*, 92, 106029. <https://doi.org/10.1016/j.bspc.2024.106029>

- [15] Zakariah, M., Al-Razgan, M., & Alfakih, T. (2024). Dual vision Transformer-DSUNET with feature fusion for brain tumor segmentation. *Heliyon*, 10, e37804. <https://doi.org/10.1016/j.heliyon.2024.e37804>
- [16] Musthafa, M. M., Mahesh, T. R., Kumar, V. V., & Guuwad, S. (2024). Enhancing brain tumor detection in MRI images through explainable AI using Grad-CAM with Resnet 50. *BMC Medical Imaging*. <https://doi.org/10.1186/s12880-024-01292-7>
- [17] Yu, Z., Li, X., Li, J., Chen, W., Tang, Z., & Geng, D. (2024). HSA-net with a novel CAD pipeline boosts both clinical brain tumor MR image classification and segmentation. *Computers in Biology and Medicine*, 170, 108039. <https://doi.org/10.1016/j.compbiomed.2024.108039>
- [18] Aboussaleh, I., Riffi, J., Mahraz, A. M., & Tairi, H. (2024). Inception-UDet: An Improved U-Net Architecture for Brain Tumor Segmentation. *Annals of Data Science*, 11(3), 831–853. <https://doi.org/10.1007/s40745-023-00480-6>
- [19] Malakouti, S. M., Menhaj, M. B., & Suratgar, A. A. (2024). Machine learning and transfer learning techniques for accurate brain tumor classification. *Clinical eHealth*, 7, 106–119. <https://doi.org/10.1016/j.ceh.2024.08.001>
- [20] Yalamanchili, S., Yenuga, P., Burla, N., Jonnadula, H., Bolem, S. C., Chirra, V. R. R., Ramana, V. M., Garnepudi, P., & Yamarthi, N. R. (2024). MRI Brain Tumor Analysis on Improved VGG16 and Efficient NetB7 Models. *Journal of Image and Graphics*, 12(1), 103-116. <https://doi.org/10.18178/joig.12.1.103-116>
- [21] Priyadarshini, P., Kanungo, P., & Kar, T. (2024). Multigrade brain tumor classification in MRI images using Fine tuned efficientnet. *e-Prime - Advances in Electrical Engineering, Electronics and Energy*, 8, 100498. <https://doi.org/10.1016/j.prime.2024.100498>
- [22] Haque, R., Hassan, M. M., Bairagi, A. K., & Islam, S. M. S. (2024). NeuroNet19: an explainable deep neural network model for the classification of brain tumors using magnetic resonance imaging data. *Scientific Reports*, 14, 1524. <https://doi.org/10.1038/s41598-024-51867-1>
- [23] Rasool, N., Bhat, J. I., Wani, N. A., Ahmad, N., & Alshara, M. (2024). TransResUNet: Revolutionizing Glioma Brain Tumor Segmentation Through Transformer-Enhanced Residual UNet. *IEEE Access*, 12, 72105-72116. <https://doi.org/10.1109/ACCESS.2024.3402947>
- [24] Hossain, S., Chakrabarty, A., Gadekallu, T. R., Alazab, M., & Piran, M. J. (2024). Vision Transformers, Ensemble Model, and Transfer Learning Leveraging Explainable AI for Brain Tumor Detection and Classification. *IEEE Journal of Biomedical and Health Informatics*, 28(3), 1261-1272. <https://doi.org/10.1109/JBHI.2023.3266614>
- [25] Iriawan, N., Pravitasari, A. A., Nuraini, U. S., Nirmalasari, N. I., Azmi, T., Nasrudin, M., Fandisyah, A. F., Fithriasari, K., Purnami, S. W., Irhamah, & Ferriastuti, W. (2024). YOLO-UNet Architecture for Detecting and Segmenting the Localized MRI Brain Tumor Image. *Applied Computational Intelligence and Soft Computing*. <https://doi.org/10.1155/2024/3819801>
- [26] C. Ozdemir and Y. Dogan, "Advancing early diagnosis of Alzheimer's disease with next-generation deep learning methods," *Biomedical Signal Processing and Control*, vol. 96, pt. B, p. 106614, 2024. doi: 10.1016/j.bspc.2024.106614.
- [27] Biswas, R., & Gini, R. J. (2024). Multi-class classification of Alzheimer's disease detection from 3D MRI images using ML techniques and its performance analysis. *Multimedia Tools and Applications*, 83, 33527-33554. <https://doi.org/10.1007/s11042-023-16519-y>
- [28] I. Ayus and D. Gupta, "A novel hybrid ensemble based Alzheimer's identification system using deep learning technique," *Biomedical Signal Processing and Control*, vol. 92, p. 106079, 2024. doi: 10.1016/j.bspc.2024.106079.
- [29] Nour, M., Senturk, U., & Polat, K. (2024). A novel hybrid model in the diagnosis and classification of Alzheimer's disease using EEG signals: Deep ensemble learning (DEL) approach. *Biomedical Signal Processing and Control*, 89, 105751. <https://doi.org/10.1016/j.bspc.2023.105751>
- [30] Ali, E. H., Sadek, S., El Nashef, G. Z., & Makki, Z. F. (2024). Advanced Integration of Machine Learning Techniques for Accurate Segmentation and Detection of Alzheimer's Disease. *Algorithms*, 17, 207. <https://doi.org/10.3390/a17050207>
- [31] Tripathy, S. K., Nayak, R. K., Gadupa, K. S., Mishra, R. D., Patel, A. K., Satapathy, S. K., Bhoi, A. K., & Barsocchi, P. (2024). Alzheimer's Disease Detection via Multiscale Feature Modelling Using Improved Spatial Attention Guided Depth Separable CNN. *International Journal of Computational Intelligence Systems*, 17, 113. <https://doi.org/10.1007/s44196-024-00502-y>
- [32] Mahmood, T., Rehman, A., Saba, T., Wang, Y., & Alamri, F. S. (2024). Alzheimer's disease unveiled: Cutting-edge multi-modal neuroimaging and computational methods for enhanced diagnosis. *Biomedical Signal Processing and Control*, 97, 106721.
- [33] Mahmud, T., Barua, K., Habiba, S.U., Sharmen, N., Hossain, M.S., & Andersson, K. (2024). An Explainable AI Paradigm for Alzheimer's Diagnosis Using Deep Transfer Learning. *Diagnostics*, 14, 345.

- [34] Matlani, P. (2024). BiLSTM-ANN: Early Diagnosis of Alzheimer's Disease Using Hybrid Deep Learning Algorithms. *Multimedia Tools and Applications*, 83, 60761-60788.
- [35] Malu, G., Uday, N., Sherly, E., Abraham, A., & Bodhey, N. K. (2024). CirMNet: A Shape-Based Hybrid Feature Extraction Technique Using CNN and CMSMD for Alzheimer's MRI Classification. *IEEE Access*, 12, 80491-80504.
- [36] Bringas, S., Duque, R., Lage, C., & Montaña, J. L. (2024). CLADSI: Deep Continual Learning for Alzheimer's Disease Stage Identification Using Accelerometer Data. *IEEE Journal of Biomedical and Health Informatics*, 28(6), 3401-3410.
- [37] Zia-ur-Rehman, Awang, M. K., Rashid, J., Ali, G., Hamid, M., Mahmoud, S. F., Saleh, D. I., & Ahmad, H. I. (2024). Classification of Alzheimer Disease Using DenseNet-201 Based on Deep Transfer Learning Technique. *PLOS ONE*, 19(9), e0304995.
- [38] Sorour, S. E., El-Mageed, A. A. A., Albarrak, K. M., Alnaim, A. K., Wafa, A. A., & El-Shafeiy, E. (2024). Classification of Alzheimer's Disease Using MRI Data Based on Deep Learning Techniques. *Journal of King Saud University - Computer and Information Sciences*, 36, 101940.
- [39] Yu, W.-Y., Sun, T.-H., Hsu, K.-C., Wang, C.-C., Chien, S.-Y., Tsai, C.-H., & Yang, Y.-W. (2024). Comparative Analysis of Machine Learning Algorithms for Alzheimer's Disease Classification Using EEG Signals and Genetic Information. *Computers in Biology and Medicine*, 176, 108621.
- [40] Song, B., & Yoshida, S. (2024). Explainability of three-dimensional convolutional neural networks for functional magnetic resonance imaging of Alzheimer's disease classification based on gradient-weighted class activation mapping. *PLOS ONE*, 19(5), e0303278. doi:10.1371/journal.pone.0303278
- [41] Alp, S., Akan, T., Bhuiyan, M. S., Disbrow, E. A., Conrad, S. A., Vanchiere, J. A., Kevil, C. G., & Bhuiyan, M. A. N. (2024). Joint transformer architecture in brain 3D MRI classification: its application in Alzheimer's disease classification. *Scientific Reports*, 14, 8996.
- [42] Qian, C., & Wang, Y. (2024). MMANet: A Multi-Task Residual Network for Alzheimer's Disease Classification and Brain Age Prediction. *IRBM*, 45, 100840. <https://doi.org/10.1016/j.irbm.2024.100840>
- [43] Mahim, S. M., Ali, M. S., Hasan, M. O., Nafi, A. A. N., Sadat, A., Hasan, S. A., Shareef, B., Ahsan, M. M., Islam, M. K., Miah, M. S., & Niu, M. B. (2024). Unlocking the Potential of XAI for Improved
- [44] Magesh, P.R., Myloth, R.D., & Tom, R.J. (2020). An Explainable Machine Learning Model for Early Detection of Parkinson's Disease using LIME on DaTSCAN Imagery. *Computers in Biology and Medicine*, 126, 104041. <https://doi.org/10.1016/j.compbimed.2020.104041>
- [45] Bhandari, N., Walambe, R., Kotecha, K., & Kaliya, M. (2023). Integrative gene expression analysis for the diagnosis of Parkinson's disease using machine learning and explainable AI. *Computers in Biology and Medicine*, 163, 107140. <https://doi.org/10.1016/j.compbimed.2023.107140>
- [46] Kumar, A., Kouznetsova, V.L., Kesari, S., & Tsigelny, I.F. (2024). Parkinson's Disease Diagnosis Using miRNA Biomarkers and Deep Learning. *Frontiers in Bioscience (Landmark Edition)*, 29(1), 4. <https://doi.org/10.31083/j.fbl2901004>
- [47] Priyadharshini, S., Ramkumar, K., Vairavasundaram, S., Narasimhan, K., Venkatesh, S., Amirtharajan, R., & Kotecha, K. (2024). A Comprehensive framework for Parkinson's disease diagnosis using explainable artificial intelligence empowered machine learning techniques. *Alexandria Engineering Journal*, 107, 568-582. <https://doi.org/10.1016/j.aej.2024.07.106>
- [48] Yildirim, M., Kiziloluk, S., Aslan, S., & Sert, E. (2024). A new hybrid approach based on AOA, CNN and feature fusion that can automatically diagnose Parkinson's disease from sound signals: PDD-AOA-CNN. *Signal, Image and Video Processing*, 18, 1227-1240. <https://doi.org/10.1007/s11760-023-02826-2>
- [49] Saleh, S., Ouhmda, A., Cherrad, B., AlSarem, M., Hamda, S., Albl, A., Mahyoob, M., & Bouattane, O. (2024). A novel hybrid CNN-KNN ensemble voting classifier for Parkinson's disease prediction from hand sketching images. *Multimedia Tools and Applications*. <https://doi.org/10.1007/s11042-024-19314-5>
- [50] Teo, Y. X., Lee, R. E., Nurzaman, S. G., Tan, C. P., & Chan, P. Y. (2024). Action tremor features discovery for essential tremor and Parkinson's disease with explainable multilayer BiLSTM. *Computers in Biology and Medicine*, 180, 108957. <https://doi.org/10.1016/j.compbimed.2024.108957>
- [51] Islam, N., Turza, M. S. A., Fahim, S. I., & Rahman, R. M. (2024). Advanced Parkinson's Disease Detection: A comprehensive artificial intelligence approach utilizing clinical assessment and neuroimaging samples. *International Journal of Cognitive Computing in Engineering*, 5, 199-220. <https://doi.org/10.1016/j.ijcce.2024.05.001>
- [52] Veetil, I. K., Chowdary, D. E., Chowdary, P. N., Sowmya, V., & Gopalakrishnan, E. A. (2024). An analysis of data leakage and generalizability in MRI based classification of Parkinson's Disease using explainable 2D Convolutional Neural Networks. *Digital Signal Processing*, 147, 104407. <https://doi.org/10.1016/j.dsp.2024.104407>

- [53] M. Mahendran and R. Visalakshi, "An ensemble of ResNet model for classification of Parkinson disease," *International Journal of Nutrition, Pharmacology, Neurological Diseases*, vol. 14, pp. 9-14, 2024. doi: 10.4103/ijnpnd.ijnpnd_22_23.
- [54] Palakayala, A. R., & Kuppasamy, P. (2024). AttentionLUNet: A Hybrid Model for Parkinson's Disease Detection Using MRI Brain. *IEEE Access*. DOI: 10.1109/ACCESS.2024.3420125
- [55] Yang, J., Williams, S., Hogg, D. C., Alty, J. E., & Relton, S. D. (2024). Deep learning of Parkinson's movement from video, without human-defined measures. *Journal of the Neurological Sciences*, 463, 123089. DOI: 10.1016/j.jns.2024.123089
- [56] Wang, H., Jiang, H., Chen, G., Du, Y., Lu, Z., Hu, Z., & Mok, G. S. P. (2024). Deep-Learning-Based Cross-Modality Striatum Segmentation for Dopamine Transporter SPECT in Parkinson's Disease. *IEEE Transactions on Radiation and Plasma Medical Sciences*, 8(7), 752-761. DOI: 10.1109/TRPMS.2024.3398360
- [57] Dentamaro, V., Impedovo, D., Musti, L., Pirlo, G., & Taurisano, P. (2024). Enhancing early Parkinson's disease detection through multimodal deep learning and explainable AI: insights from the PPMI database. *Scientific Reports*, 14, 20941. DOI: 10.1038/s41598-024-70165-4
- [58] Al-Tam, R. M., Hashim, F. A., Maqsood, S., Abualigah, L., & Alwhaibi, R. M. (2024). Enhancing Parkinson's Disease Diagnosis Through Stacking Ensemble-Based Machine Learning Approach. *IEEE Access*, 12, 79549-79567. DOI: 10.1109/ACCESS.2024.3408680
- [59] Desai, S., Chhinkaniwala, H., Shah, S., & Gajjar, P. (2024). Enhancing Parkinson's Disease Diagnosis through Deep Learning-Based Classification of 3D MRI Images. *Procedia Computer Science*, 235, 201-213. DOI: 10.1016/j.procs.2024.04.023
- [60] Rao, B. S., Gopal, V. N., Akash, V., & Nazeer, S. (2024). Speed of Diagnosis for Brain Diseases Using MRI and Convolutional Neural Networks. In *Proceedings of Data Analytics and Management (ICDAM 2023)* (pp. 501–514). Springer. https://doi.org/10.1007/978-981-99-6544-1_38
- [61] Chen, A., Lin, D., & Gao, Q. (2024). Enhancing brain tumor detection in MRI images using YOLO-NeuroBoost model. *Frontiers in Neurology*, 15. <https://doi.org/10.3389/fneur.2024.1445882>
- [62] N. Ravi et al., "Sam 2: Segment anything in images and videos," arXiv preprint arXiv:2408.00714, 2024.
- [63] A. Rostami, "Labeled MRI Brain Tumor Dataset," Roboflow Universe, 2024.
- [64] Deep Learning, "Alzheimer's Disease Detection Dataset," Roboflow Universe, 2023.
- [65] MiddleBrain, "Parkinson Disease Dataset," Roboflow Universe, 2024.
- [66] Gonzalez, R. C., & Woods, R. E. (2018). *Digital Image Processing* (4th ed.). Pearson.
- [67] Burger, W., & Burge, M. J. (2016). *Digital Image Processing: An Algorithmic Introduction Using Java* (2nd ed.). Springer. <https://doi.org/10.1007/978-1-4471-6684-9>
- [68] Zuiderveld, K. (1994). Contrast Limited Adaptive Histogram Equalization. In P. S. Heckbert (Ed.), *Graphics Gems IV* (pp. 474–485). Academic Press.
- [69] Shorten, C., & Khoshgoftaar, T. M. (2019). A survey on image data augmentation for deep learning. *Journal of Big Data*, 6(1), 60. <https://doi.org/10.1186/s40537-019-0197-0>
- [70] D. P. Kingma and J. Ba, "Adam: A method for stochastic optimization," arXiv preprint arXiv:1412.6980, 2014.
- [71] Powers, D. M. (2020). Evaluation: From Precision, Recall, and F-measure to ROC, Informedness, Markedness & Correlation. *Journal of Machine Learning Technologies*, 2(1), 37–63.
- [72] Saito, T., & Rehmsmeier, M. (2015). The Precision-Recall Plot Is More Informative than the ROC Plot When Evaluating Binary Classifiers on Imbalanced Datasets. *PLoS ONE*, 10(3), e0118432.
- [73] Everingham, M., Van Gool, L., Williams, C. K., Winn, J., & Zisserman, A. (2010). The Pascal Visual Object Classes (VOC) Challenge. *International Journal of Computer Vision*, 88(2), 303–338.
- [74] Lin, T. Y., Maire, M., Belongie, S., Hays, J., Perona, P., Ramanan, D., & Dollár, P. (2014). Microsoft COCO: Common Objects in Context. In *Proceedings of the European Conference on Computer Vision (ECCV)* (pp. 740–755).
- [75] E. Logeswaran and M. El-Sayed, "Magnetic resonance imaging of brain tumors," *International Journal of Biomedical Imaging*, 2014.
- [76] J. Redmon and A. Farhadi, "YOLOv3: An incremental improvement," arXiv preprint arXiv:1804.02767, 2018.
- [77] A. Kirillov et al., "Segment Anything," arXiv preprint arXiv:2304.02643, 2023.
- [78] J. A. Hartigan, "Representation of multidimensional data by color mappings," *Journal of the American Statistical Association*, vol. 77, no. 379, pp. 604-614, 1982.
- [79] Redmon, J., Farhadi, A.: YOLOv3: An Incremental Improvement. arXiv preprint arXiv:1804.02767 (2018).
- [80] Liu, W., Anguelov, D., Erhan, D., Szegedy, C., Reed, S., Fu, C.-Y., Berg, A.C.: SSD: Single Shot MultiBox Detector. In: *Computer Vision – ECCV 2016*, pp. 21–37. Springer, Cham (2016). https://doi.org/10.1007/978-3-319-46448-0_2

- [81] Ulku, I., Akagunduz, E.: A Survey on Deep Learning-Based Architectures for Semantic Segmentation on 2D Images. In: Applied Intelligence, vol. 51, no. 5, pp. 3017–3041 (2021). <https://doi.org/10.1007/s10489-020-01910-y>
- [82] Ronneberger, O., Fischer, P., Brox, T.: U-Net: Convolutional Networks for Biomedical Image Segmentation. In: Medical Image Computing and Computer-Assisted Intervention – MICCAI 2015, pp. 234–241. Springer, Cham (2015). https://doi.org/10.1007/978-3-319-24574-4_28
- [83] Zhou, Z., Siddiquee, M.M.R., Tajbakhsh, N., Liang, J.: UNet++: Redesigning Skip Connections to Exploit Multiscale Features in Image Segmentation. IEEE Transactions on Medical Imaging 39(6), 1856–1867 (2020). <https://doi.org/10.1109/TMI.2019.2959609>
- [84] Wang, A., Chen, H., Liu, L., Chen, K., Lin, Z., Han, J., & Ding, G. (2024). Yolov10: Real-time end-to-end object detection. arXiv preprint arXiv:2405.14458.